

Theory of electric, magnetic, and toroidal polarizations in crystalline solids with applications to hexagonal lonsdaleite and cubic diamond*

R. Winkler^{1,2} and U. Zülicke³

¹*Department of Physics, Northern Illinois University, DeKalb, Illinois, 60115, USA*

²*Materials Science Division, Argonne National Laboratory, Lemont, Illinois 60439, USA*

³*MacDiarmid Institute, School of Chemical and Physical Sciences,*

Victoria University of Wellington, PO Box 600, Wellington 6140, New Zealand

(Dated: April 6, 2023)

Multipolar order in bulk crystalline solids is characterized by multipole densities — denoted as *polarizations* in this work — that cannot be cleanly defined using the concepts of classical electromagnetism. Here we use group theory to overcome this difficulty and present a systematic study of electric, magnetic, and toroidal multipolar order in crystalline solids. Based on our symmetry analysis, we identify five categories of polarized matter, each of which is characterized by distinct features in the electronic band structure. For example, Rashba spin splitting in electropolar bulk materials like wurtzite represents the electric dipolarization in these materials. We also develop a general formalism of indicators for individual multipole densities that provide a physical interpretation and quantification of multipolar order. Our work clarifies the relation between patterns of localized multipoles and macroscopic multipole densities they give rise to. To illustrate the general theory, we discuss its application to polarized variants of hexagonal lonsdaleite and cubic diamond structures. Our work provides a general framework for classifying and expanding current understanding of multipolar order in complex materials.

I. INTRODUCTION

It is well-known that a proper definition of electric dipolarization as a bulk property is nontrivial [1, 2]. The naive electromagnetic definition of electric dipolarization as the dipole moment of a unit cell is unsatisfactory as this quantity generally depends on the arbitrary choice of a unit cell [3]. Thus a proper description of the electromagnetic properties of solids requires tools beyond those supplied by classical electrodynamics.

Important progress has been made by introducing the modern theories of electric dipolarization and magnetization where geometric phases are used to quantify these dipole densities (multipole order $\ell = 1$) independently of the choice of unit cell [1, 2, 4, 5]. Within the modern theory, the electric dipolarization has a clear physical interpretation relative to a reference state. However, for systems showing a spontaneous electric dipolarization, the interpretation and observability of this quantity have remained ambiguous. Also, it is a significant challenge to extend the modern-theory approaches to multipole densities of higher multipole order $\ell > 1$ [6].

Even before the advent of the modern theories, some early studies did not make any reference to electromagnetism in their investigation of dipolarizations in materials, as they recognized how crystal symmetry allows one to identify crystal structures that permit a bulk electric dipolarization (so-called polar crystals include pyroelectric and ferroelectric media [7–9]) or a bulk magnetization (ferromagnetic crystals [10–12]). According to Neumann’s principle (see Refs. [7, 8] for seminal discussions), the crystal classes can be rigorously divided into

those that permit a macroscopic electric dipolarization or magnetization, and those for which these phenomena are forbidden. Magnetic crystal classes that do not permit a magnetization have been generically associated with antiferromagnetism [12].

The approach pursued in the present work overcomes the unsatisfactory electromagnetic definition of electric and magnetic multipole densities that is inadequate for crystalline solids; we rely entirely on symmetry to extend the notion of bulk dipolarization and magnetization to electric and magnetic multipole densities of higher orders $\ell > 1$. To this end, we treat the black-white symmetries space inversion symmetry (SIS) and time inversion symmetry (TIS) on the same footing [13]. Moreover, we treat electric and magnetic order on the same footing. Our systematic theory provides a broader framework for recent efforts to study electric and magnetic multipolar order in solids [14–18] and lends itself for wider application in the context of complex materials [19–24]. Throughout this work, we focus on systems that are in thermal equilibrium, thus leaving aside the interesting topic of current-induced multipolar order [25].

In the following, the term *polarization* refers to a gen-

TABLE I. Signature ss' of multipoles of order ℓ . The four different types of multipoles arising for any given ℓ are associated with the respective irreducible representations $D_\ell^{ss'}$ of the full rotation group $R_{i \times \theta} \equiv R \times C_{i \times \theta}$, where $R \equiv SO(3)$ is the proper rotation group.

	electric	magnetic	electro-toroidal	magneto-toroidal
ℓ even	++	--	–+	+–
ℓ odd	–+	+–	++	--

* Dedicated to E. I. Rashba on the occasion of his 95th birthday.

TABLE II. Families of electric, magnetic, and toroidal multipole densities (*polarizations*) of order ℓ permitted by SIS, TIS and CIS. Symmetry operations present (absent) in a given inversion group are labeled “•” (“o”). Polarizations that are allowed (forbidden) under an inversion group are likewise labeled “•” (“o”). We also list the signature ss' for each family of polarizations, with $s = \pm$ ($s' = \pm$) indicating transformation behavior under space inversion i (time inversion θ). Each inversion group defines a category of polarized matter, as indicated in the last column.

inversion group	symmetry i θ $i\theta$			electric		magnetic		electrotoroidal		magnetotoroidal		category of polarized matter
				ℓ even	ℓ odd	ℓ even	ℓ odd	ℓ even	ℓ odd	ℓ even	ℓ odd	
				++	-+	--	+-	-+	++	+-	--	
$C_{i \times \theta} = \{e, i, \theta, i\theta\}$	•	•	•	•	o	o	o	•	o	o	parapolar (PP)	
$C_\theta = \{e, \theta\}$	o	•	o	•	•	o	o	•	•	o	electropolar (EP)	
$C_i = \{e, i\}$	•	o	o	•	o	o	•	o	•	•	magnetopolar (MP)	
$C_{i\theta} = \{e, i\theta\}$	o	o	•	•	o	•	o	o	•	o	antimagnetopolar (AMP)	
$C_1 = \{e\}$	o	o	o	•	•	•	•	•	•	•	multipolar (MuP)	

eral realization of bulk multipolar order with $\ell \geq 0$. Four types of polarizations — electric, magnetic, electrotoroidal, and magnetotoroidal — are presented in Table I. The *signature* ss' indicates how a polarization behaves under space inversion (even/odd if $s = +/-$) and time inversion (even/odd if $s' = +/-$). The electric (magnetic) polarization of order $\ell = 1$ corresponds to the electric dipolarization (magnetization), having signature $-+$ ($+-$). This general group-theoretical definition of electric and magnetic multipolar order is independent of the arbitrary choice of a unit cell. It is also independent of a material’s electrodynamic properties and, therefore, applies to both insulators and metals.

A comprehensive classification of ways to combine polarizations is based on their transformation behavior under SIS, TIS, and the combined inversion symmetry (CIS) represented by the operations i , θ , and $i\theta$, respectively. Five distinct inversion groups can be formed from these symmetry operations, as defined in Table II, where we also indicate which polarizations are permitted under these groups. The only types of polarizations permitted under the full inversion group $C_{i \times \theta} \equiv C_i \times C_\theta$ are even- ℓ electric polarizations called *parapolarizations*, and we label the associated matter category *parapolar*. On the opposite extreme, the trivial inversion group C_1 containing only the identity e as a symmetry element allows all polarization types, and we label the category of polarized matter associated with C_1 *multipolar*. Each of the remaining inversion groups contains strictly one inversion operation i , θ , or $i\theta$ as a symmetry element. As a result, only a single type of electric or magnetic polarization is symmetry-allowed: odd- ℓ *electropolarizations* for the time inversion group C_θ , odd- ℓ *magnetopolarizations* for the space inversion group C_i , and even- ℓ *antimagnetopolarizations* for the combined inversion group $C_{i\theta}$. Our unified treatment reveals a far-reaching correspondence between electric and magnetic order in crystalline solids.

Our theory enables us to identify measurable *indicators* that signal the presence of electric and magnetic order in the electronic band structure. Some of these indicators

are quite familiar, though their relation to electric and magnetic order was not established previously.

A classical example for a bulk crystal with a spontaneous electric dipolarization is wurtzite [26, 27]. Wurtzite is also the classical example for a bulk crystal showing the Rashba effect [28]. Generally, the Rashba effect is characterized by a term $\alpha \cdot (\mathbf{k} \times \boldsymbol{\sigma})$, where $\hbar\mathbf{k}$ is crystal momentum and the vector $\boldsymbol{\sigma}$ of Pauli spin matrices represents the spin degree of freedom of the Bloch electrons [29]. By definition, the Rashba effect is proportional to a polar vector α . In confined geometries, the vector α is commonly associated with a built-in, or external, electric field that controls the magnitude of the Rashba effect [30, 31]. In bulk materials like wurtzite, no such intuitive picture exists for the vector α , and its physical meaning has remained unclear [28, 32]. The Rashba effect exists in all bulk crystal structures that belong to one of the ten polar crystal classes [8]. We argue that, in these structures, the vector α represents the bulk dipolarization ($\ell = 1$). The Rashba effect is thus a measure of the spontaneous electric dipolarization in bulk wurtzite structures and other polar crystals. Similarly, the Dresselhaus term [33] in bulk zincblende structures represents an electric octupolarization ($\ell = 3$), and Dresselhaus spin splitting provides a measure of the spontaneous electric octupolarization in bulk zincblende structures.

In finite systems such as molecules, only the lowest- ℓ nonvanishing electric and magnetic multipoles are well-defined because higher-order multipoles depend on the choice of origin of the coordinate systems [34, 35]. This problem is closely related to the problem described above, where, for infinite crystalline solids, even the multipole density of lowest nonvanishing order cannot be identified with the multipole moment of a unit cell because this moment depends on the arbitrary definition of the unit cell. We show that multipole densities in crystalline solids must, indeed, be divided into four *families* representing even- ℓ and odd- ℓ electric and magnetic multipoles. Within each family, only the lowest-order multipole density is well-defined. But even- ℓ electric (magnetic) multipole densities can be defined independent of

TABLE III. Magnetic point groups of electrically and magnetically polarized variations of lonsdaleite and diamond. Starting from a pristine crystal structure (lonsdaleite or diamond) that is compatible with an even-parity electric polarization ($\ell = 2$ in lonsdaleite and $\ell = 4$ in diamond), its symmetries are broken by electric and/or magnetic polarizations as indicated. We use an extended Schönflies notation [13] where minor groups with respect to space inversion i , time inversion θ , and their combination $i\theta$ are denoted by $G\{\tilde{G}\}$, $G(\tilde{G})$ and $G\{\tilde{G}\}$, respectively. The symbols C_i , C_θ and $C_{i\theta}$ denote the order-2 groups associated with i , θ and $i\theta$, and $C_{i\times\theta} \equiv C_i \times C_\theta$ is the full inversion group. Expressions on the right-hand side of an "=" sign reveal how the black-white symmetries i , θ and $i\theta$ are combined with proper rotations [13].

polarization	ss'	category	Lonsdaleite family	Diamond family
$\ell = 4$ electric	++	PP		$O_h \times C_\theta = O \times C_{i\times\theta}$ (diamond)
magnetic	--	AMP	$D_{6h}(D_{3h}) = D_6(D_3) \times C_{i\theta}$	$O_h(O) = O \times C_{i\theta}$
$\ell = 3$ electric	-+	EP	$D_{3h} \times C_\theta = D_6[D_3] \times C_\theta$	$T_d \times C_\theta = O[T] \times C_\theta$ (zincblende)
magnetic	+−	MP	$D_{6h}(D_{3d}) = D_6(D_3) \times C_i$	$O_h(T_h) = O(T) \times C_i$
$\ell = 2$ electric	++	PP	$D_{6h} \times C_\theta = D_6 \times C_{i\times\theta}$ (lonsdaleite)	$D_{4h} \times C_\theta = D_4 \times C_{i\times\theta}$ (strain)
magnetic	--	AMP		$D_{4h}(D_{2d}) = D_4(D_2) \times C_{i\theta}$
electric magnetic	--	AMP	$D_{6h}(D_6) = D_6 \times C_{i\theta}$	$D_{4h}(D_{2d}) = D_4(D_2) \times C_{i\theta}$
electric \perp magnetic	--	AMP	$D_{2h}(C_{2v}) = D_2(C_2) \times C_{i\theta}$	$D_{2h}(C_{2v}) = D_2(C_2) \times C_{i\theta}$
$\ell = 1$ electric	-+	EP	$C_{6v} \times C_\theta = D_6[C_6] \times C_\theta$ (wurtzite)	$C_{4v} \times C_\theta = D_4[C_4] \times C_\theta$
magnetic	+−	MP	$D_{6h}(C_{6h}) = D_6(C_6) \times C_i$	$D_{4h}(C_{4h}) = D_4(C_4) \times C_i$

odd- ℓ electric (magnetic) multipole densities.

Atomic multipoles can act as microscopic building blocks for macroscopic multipolar order, including higher-order atomic magnetic multipoles beyond magnetic dipoles [36]. We demonstrate that the order and orientation of these local multipoles are fixed by site symmetries that are tabulated for all crystallographic space groups [37, 38]. But the order of the local multipoles proves to not be simply related to the order ℓ of the macroscopic multipole densities they generate. For example, in diamond structures, atomic sp^3 hybrid orbitals form local electric octupoles whose configuration results in a macroscopic hexadecapolarization with $\ell = 4$.

Toroidal order has been viewed as an essential complement to electric and magnetic multipolar order [39–43]. However, the physical significance of toroidal moments is being debated [44]. Our work clarifies the role of toroidal order in solids. Under the full rotation group $R_{i\times\theta} \equiv R \times C_{i\times\theta}$, where $R \equiv SO(3)$ is the proper rotation group, toroidal moments are fundamentally distinct from electric and magnetic multipoles, where these moments transform according to different irreducible representations (IRs) of $R_{i\times\theta}$ (Table I). This distinction is lost in a crystalline environment, where the IRs of $R_{i\times\theta}$ representing toroidal moments are mapped onto the same finite set of IRs of the crystallographic point groups as the IRs of $R_{i\times\theta}$ representing electric and magnetic multipoles. Therefore, the observable physics one can associate with toroidal moments in crystalline solids is indistinguishable from the physics due to electric and magnetic multipoles.

We illustrate our general theory taking polarized variations of lonsdaleite and diamond as examples; two highly symmetric crystal structures whose variations are realized in numerous technologically relevant materials. An overview of the specific types of crystal structures considered in the present work is presented in Table III.

The space-inversion and time-inversion symmetric pristine lonsdaleite and diamond structures are compatible with even- ℓ electric polarizations of order $\ell \geq 2$ for lonsdaleite and $\ell \geq 4$ for diamond, respectively [45]. Introduction of odd- ℓ electric polarizations (also $\ell = 2$ in diamond) and even- or odd- ℓ magnetic polarizations reduce the crystal symmetries to those specified by the magnetic point groups [13, 46] given in Table III. For example, SIS of the lonsdaleite structure is broken in the wurtzite structure with an $\ell = 1$ electropolarization (i.e., an electric dipolarization). Similarly, the zincblende structure constitutes a broken-SIS diamond structure due to an $\ell = 3$ electropolarization (i.e., an electric octupolarization). We also consider the structures where TIS is broken instead of SIS by introducing different magnetic polarizations ranging from $\ell = 1$ to $\ell = 4$. Lonsdaleite and diamond structures with a magnetic quadrupolarization ($\ell = 2$) or hexadecapolarization ($\ell = 4$) are antiferromagnets [47] that break both SIS and TIS individually but preserve CIS.

The remainder of this article is organized as follows. We start by developing the general theory in Sec. II. Results obtained from application of the theory to crystal structures from the lonsdaleite and diamond families are presented in the subsequent Secs. III and IV, respectively. Each main section has a preamble that gives a more detailed overview of the topics discussed there. Conclusions and a brief outlook are presented in Sec. V.

II. GENERAL THEORY

In this section, we develop a rigorous theory of multipolar order in crystalline solids based on group theory. The symmetry properties of electric and magnetic multipoles in free space are discussed in Sec. II A, with special

focus on their classification according to transformation behavior under space inversion i and time inversion θ . Section II B considers multipole *densities* in crystalline solids, which we refer to as *polarizations*. Five distinct categories of polarized matter are identified. Sections II C and II D develop the mathematical tools required to enable the derivation of distinctive *indicators* for multipolar order in Sec. II E. The consideration of symmetry hierarchies in Sec. II F provides a platform for addressing the subtle issue of when and how coexisting multipole densities can be properly defined in a solid. Section II G identifies distinctive band-structure features for each category of polarized matter. Toroidal moments are discussed in Sec. II H. The final Sec. III elucidates the relationship between macroscopic multipole densities in a solid's bulk and microscopic multipoles localized on atomic sites.

A. Multipoles

We are interested in electric and magnetic multipolar order in a crystalline environment. In free space, electric and magnetic multipoles \mathcal{M} of order ℓ can be viewed as spherical tensors that transform irreducibly under the rotation group $R_{i \times \theta}$ [48], i.e., they can be classified by the $(2\ell + 1)$ -dimensional IRs $D_\ell^{ss'}$ ($\ell = 0, 1, 2, \dots$) of $R_{i \times \theta}$ according to which these quantities transform [34, 49, 50]. Below we distinguish the components of these $(2\ell + 1)$ -dimensional IRs via an index m in the usual way [49, 50].

The *signature* ss' indicates how a quantity behaves under space inversion (even/odd if $s = +/-$) and time inversion (even/odd if $s' = +/-$). For even ℓ , electric (magnetic) multipoles transform according to the IR D_ℓ^{++} (D_ℓ^{--}) of $R_{i \times \theta}$, while for odd ℓ , electric (magnetic) multipoles transform according to D_ℓ^{-+} (D_ℓ^{+-}), see Table I. Thus even- ℓ electric multipoles preserve both SIS and TIS, whereas even- ℓ magnetic multipoles break both SIS and TIS, but the combined inversion $i\theta$ remains a good symmetry. Odd- ℓ electric (magnetic) multipoles break SIS (TIS). The distinct behavior of these multipoles under SIS and TIS suggests to divide these multipoles into four *families* representing even- ℓ and odd- ℓ electric and magnetic multipoles.

The behavior of the four families of electric and magnetic multipoles under SIS and TIS can be classified via the five *inversion groups* $C_{i \times \theta}$, C_θ , C_i , $C_{i\theta}$ and C_1 that can be formed from space inversion i and time inversion θ . (See the explicit definitions given in the left column of Table II.) Under the full inversion group $C_{i \times \theta}$, when i and θ are independently good symmetries, only even- ℓ electric multipoles (signature $++$) are allowed. Under C_θ , i.e., when i is broken, we may also have odd- ℓ electric multipoles ($-+$). Under C_i , on the other hand, i.e., when θ is broken, we may have instead odd- ℓ magnetic multipoles ($+-$). When both i and θ are broken, but $i\theta$ remains a good symmetry so that we get the group $C_{i\theta}$, we may have even- ℓ magnetic multipoles ($--$). Even- ℓ and odd- ℓ electric and magnetic multipoles (all signatures

ss') are allowed simultaneously if none of the operations i , θ , and $i\theta$ represent good symmetries, i.e., we get the trivial group C_1 that only contains the identity e .

B. Categories of polarized matter

An extended crystal must be characterized in terms of multipole *densities* \mathbf{m} instead of multipoles \mathcal{M} . To emphasize the conceptual difference between the quantities \mathbf{m} , which constitute a macroscopic property of the bulk material, and the localized multipoles \mathcal{M} characterizing, e.g., molecules [34, 35], we refer to \mathbf{m} as a *polarization*. Nonetheless, from the perspective of group theory, both \mathcal{M} and \mathbf{m} are spherical tensors of order ℓ that share the same transformation properties under the point-group symmetries discussed here. The multipoles \mathcal{M} of localized systems such as molecules can be characterized in terms of the point groups G characterizing these systems [51]. Similarly, in a crystalline environment, the symmetry is reduced compared with free space. According to Neumann's principle, the relevant symmetry group for material tensors such as multipole densities is the crystallographic point group G defining the crystal class of a crystal structure [7, 8, 52]. These groups are finite subgroups of the rotation group $R_{i \times \theta}$.

In total, 122 magnetic crystallographic point groups G can be formed [10, 12, 53]. To categorize these groups, we expand on the classification of multipolar order based on the inversion symmetries $\gamma = i, \theta, \text{ and } i\theta$. We decompose

$$G = \tilde{G} \times C_\gamma, \quad (1)$$

where \tilde{G} denotes the proper or improper subgroup of G that contains none of the inversion symmetries γ as individual group elements, and C_γ is the inversion group that can be formed from the inversion symmetries γ that appear as group elements in G . In this way we identify five qualitatively distinct categories of *macroscopic* electromagnetic multipolar order based on the five inversion groups C_γ [54]. The five categories are listed in the last column of Table II, and their properties are as follows.

(i) The full inversion group $C_{i \times \theta}$ defines *parapolar* systems that have the highest symmetry. Even- ℓ electric multipole densities (signature $++$) are the only electromagnetic multipole densities permitted by $C_{i \times \theta}$, and we use the label *parapolarization* for members of this family. Parapolar systems are thus both paraelectric and paramagnetic.

(ii) The non-cyclic group $C_{i \times \theta}$ has order 4. It is isomorphic to the Klein four-group in abstract group theory [13]. Accordingly, the group $C_{i \times \theta}$ has three order-2 subgroups C_θ , C_i , and $C_{i\theta}$ that represent mutually exclusive alternatives to reduce the symmetry of parapolar systems. We elaborate on each one of these in turn. (ii-a) The group C_θ defines *electropolar* systems that may possess odd- ℓ electric multipole densities (signature $-+$, any member of this family is labeled an *electropolarization*), including an electric dipole density (an electric dipolarization with

$\ell = 1$). Therefore, electropolar systems include, e.g., pyroelectrics and ferroelectrics [7, 8, 55, 56]. (ii-b) The group C_i defines *magnetopolar* systems that may possess odd- ℓ magnetic multipole densities (a *magnetopolarization*, $+-$), including a magnetic dipole density (a magnetization with $\ell = 1$). Therefore, magnetopolar systems include, e.g., ferromagnets [11, 12, 55, 57]. (ii-c) The group $C_{i\theta}$ defines *antimagnetopolar* systems that may possess even- ℓ magnetic multipole densities (an *antimagnetopolarization*, $--$). Antiferromagnets can be antimagnetopolar or magnetopolar as illustrated below [58]. We denote the electropolar, magnetopolar and antimagnetopolar groups jointly as *unipolar* groups.

(iii) The trivial inversion group C_1 defines *multipolar* systems that may possess electric and magnetic multipole densities of any order ℓ (all signatures ss') so that they can be simultaneously electropolar and (anti-)magnetopolar. Multipolar systems include, e.g., multiferroics [59, 60].

The five inversion groups C_γ treat the black-white symmetries i and θ on the same footing. Closely related, the five categories in Table II treat electric and magnetic order on the same footing. Here we complement the standard Schönflies notation for magnetic point groups [13, 46] with the corresponding expressions according to Eq. (1) that reveal how the inversion operations are combined with proper rotations.

C. Compatibility relations

The crystallographic point groups G are finite subgroups of the rotation group $R_{i \times \theta}$, and the IRs $D_\ell^{ss'}$ of $R_{i \times \theta}$ can be mapped onto the IRs Γ_α of G

$$R_{i \times \theta} \mapsto G : D_\ell^{ss'} \mapsto \sum_\alpha \Gamma_\alpha. \quad (2)$$

Ignoring TIS, i.e., considering only the nonmagnetic crystallographic point groups, the *compatibility relations* (2) were tabulated up to rank $\ell = 6$ by Koster *et al.* [45, 61]. These relations indicate how spherical tensors \mathbf{m} decompose into components \mathbf{m}_α^G transforming irreducibly (IR Γ_α) under a crystallographic point group G

$$\mathbf{m} = \sum_\alpha \mathbf{m}_\alpha^G. \quad (3)$$

For brevity of notation, we ignore in Eqs. (2) and (3) that there may be multiple irreducible components \mathbf{m}_α^G transforming according to the same IR Γ_α . (This is expressed by the multiplicities with which an IR Γ_α of G is contained in an IR $D_\ell^{ss'}$ of $R_{i \times \theta}$.) The components \mathbf{m}_α^G can be obtained by projecting \mathbf{m} onto the IRs Γ_α of G . The IRs of the crystallographic point groups are at most three-dimensional, i.e., spherical multipole densities \mathbf{m} of order $\ell \geq 2$ decompose into multiple irreducible components under all crystallographic point groups G .

We make extensive use of Koster's tables [45], though occasionally we need to deviate from Koster's conventions regarding the choice of coordinate systems used to define the group elements and basis functions. Koster *et al.* define the IRs for the 32 nonmagnetic crystallographic point groups G via their characters and representative basis functions. Koster *et al.* consider only SIS but not TIS, and they use a single superscript $s = \pm$ to denote IRs that are even or odd under SIS. So-called type-III magnetic point groups [53] are isomorphic to nonmagnetic point groups (provided we do not consider double groups [62], as appropriate for Neumann's principle [52]). However, in order to identify representative basis functions for the IRs as tabulated by Koster *et al.* [45], we consider the IRs of the respective nonmagnetic subgroups of the type-III magnetic groups. Below we indicate these homomorphisms relating the magnetic groups with their nonmagnetic subgroups via an arrow, e.g., $R_{i \times \theta} \rightarrow R_i \equiv R \times C_i$. The approach followed here is thus similar to how TIS can be taken into account for nonmagnetic systems, starting with the representations of point groups ignoring TIS and subsequently incorporating the effect of TIS [52].

If the symmetry of a "parent" crystalline environment is reduced from a group G to a subgroup U of G , the IRs Γ_α of G can likewise be mapped onto the IRs Γ_β of U [63]

$$G \mapsto U : \Gamma_\alpha \mapsto \sum_\beta \Gamma_\beta. \quad (4)$$

The compatibility relations for the IRs of the crystallographic point groups have also been tabulated by Koster *et al.* [45]. They imply that, similar to Eq. (3), components \mathbf{m}_α^G of a multipole density \mathbf{m} that transform irreducibly under G can be decomposed into components \mathbf{m}_β^U that transform irreducibly under $U \subset G$

$$\mathbf{m}_\alpha^G = \sum_\beta \mathbf{m}_\beta^U. \quad (5)$$

The decomposition of a (spherical or cartesian) material tensor \mathbf{T} into its irreducible components under a point group G enables one to determine which components of \mathbf{T} are allowed to be nonzero according to crystal symmetry. Components of a material tensor \mathbf{T} are allowed by crystal symmetry [52] if these components transform according to the identity (unit) representation of G (always denoted Γ_1 in Koster's notation [45]). For higher-rank cartesian tensors with multiple indices, additional constraints for nonzero tensor components may arise from symmetry under permutation of indices. Nonzero tensor components for a range of common material tensors have been tabulated for the 32 nonmagnetic crystallographic point groups in, e.g., Refs. [8, 55, 56]. Material tensors have been discussed for the magnetic crystallographic point groups in, e.g., Refs. [55–57].

The criterion for nonzero tensor components implies that more tensor components become allowed to be nonzero if the symmetry of a system is reduced, e.g., via external perturbations or due to a phase transition [13]. This can be derived in detail from the compatibility relations between the IRs of the crystallographic point groups [45]. These techniques have been exploited earlier to study and characterize material tensors [8].

The above considerations apply, in particular, to electric and magnetic multipole densities \mathbf{m} . The decomposition (3) can be performed for multipole densities of any order ℓ and any crystallographic point group G [45]. However, \mathbf{m} remains forbidden by symmetry unless the decomposition (3) includes the identity representation Γ_1 of G .

Phrased differently, suppose a crystal structure has a group G that requires $\mathbf{m} = \mathbf{0}$ for a given multipole density of order ℓ , so that Eq. (3) does not include a term associated with Γ_1 . If the multipole density \mathbf{m} becomes nonzero (e.g., because of external perturbations or due to a phase transition), the symmetry of the system is reduced from G to a subgroup U of G that is *defined* by the condition that the nonzero component of \mathbf{m} denoted m_1^U transforms irreducibly according to the identity representation Γ_1 of U , i.e., m_1^U is a scalar under U [64]. Again, we ignore for brevity of notation that \mathbf{m} may contain multiple distinct components that transform according to Γ_1 of U . We call m_1^U the scalar of the multipole density \mathbf{m} under U .

The subgroup $U \subset G$ generally depends on which component of \mathbf{m} has become nonzero. For electric and magnetic dipole densities, the resulting subgroups U have likewise been tabulated by Koster *et al.* [45]. Groups permitting a macroscopic electric dipole density ($\ell = 1$) have previously been called polar [8], and groups permitting a magnetic dipole density (magnetization) represent ferromagnetism [11, 12, 55, 57]. According to Neumann’s principle, the respective point groups G can be identified via the criterion that the compatibility relation (2) for the IR D_1^{-+} (D_1^{+-}) of the electric (magnetic) dipole density includes the identity representation Γ_1 of G . More explicitly, we obtain the nonzero component m_1 of \mathbf{m} by projecting \mathbf{m} onto Γ_1 of G [52].

More generally, we can classify the crystallographic point groups G based on the lowest-order electric ($\ell_{\min}^{(e,\lambda)}$) and magnetic ($\ell_{\min}^{(m,\lambda)}$) multipole densities permitted in a crystal structure by its point group G (ignoring the electric monopole density transforming according to D_0^{++} that is always allowed) [45]. The superscript λ distinguishes between the lowest even ($\lambda = g$) and odd ($\lambda = u$) orders ℓ corresponding to the different families of polarizations. Generally, the higher the symmetry of a system is (as characterized via its group G), the higher are the orders $\ell_{\min}^{(e,\lambda)}$ and $\ell_{\min}^{(m,\lambda)}$, with $\ell_{\min}^{(e,u)} = \infty$ when SIS is a good symmetry and $\ell_{\min}^{(m,\lambda)} = \infty$ for nonmagnetic groups. The quantities $\ell_{\min}^{(e,\lambda)}$ and $\ell_{\min}^{(m,\lambda)}$ thus define a physically motivated hierarchy among the crystallographic point groups

G . This symmetry-based classification of macroscopic electric and magnetic order is independent of how the order is realized microscopically. For example, as discussed in Sec. IV A, an sp^3 tight-binding (TB) model can describe macroscopic electric hexadecapole densities ($\ell = 4$), and locally alternating magnetic dipoles can give rise to quadrupolar magnetic order (Secs. III F and IV H).

As per the definition of $\ell_{\min}^{(e,\lambda)}$ and $\ell_{\min}^{(m,\lambda)}$, a group G may also permit electromagnetic multipole densities of higher order than $\ell_{\min}^{(e,\lambda)}$ and $\ell_{\min}^{(m,\lambda)}$. However, it is well-known for finite, localized systems that the higher-order multipoles are generally not well-defined [34, 35]. We discuss this point in greater detail in the context of bulk multipole densities of crystalline solids in Sec. II F.

D. Theory of invariants

The theory of invariants [31, 52, 65] provides a systematic framework to describe the dynamics of Bloch electrons in the presence of perturbations such as electric and magnetic multipole densities. For conceptual clarity we restrict the discussion in the present work to nondegenerate bands, though it is well-known how the theory of invariants can be extended to bands involving degeneracies [31, 52]. We consider a system with crystallographic magnetic point group G . The general arguments presented in this section apply to any crystallographic point group G . Later on, we focus specifically on $G = D_{6h} \times C_\theta$ (lonsdaleite) and $G = O_h \times C_\theta$ (diamond). Note that these two groups constitute the highest-symmetry crystallographic point groups. All nonmagnetic crystal structures have point groups that are proper or improper subgroups of D_{6h} or O_h (ignoring TIS; see Fig. 5 in Ref. [45]), and we get subgroups of $D_{6h} \times C_\theta$ and $O_h \times C_\theta$ for magnetic structures.

The theory of invariants is based on the fact that the Hamiltonian must transform according to the identity representation Γ_1 of G . More generally, *any* operator transforming according to Γ_1 of G has a nonzero expectation value (unless the system possesses “hidden symmetries” so that G is not actually the symmetry group of the system). In contrast, the expectation values of operators not transforming according to Γ_1 of G must vanish.

In the theory of invariants, the Hamiltonian is built up from invariants that transform each according to the identity representation Γ_1 of G . Such invariants can be expressed in terms of scalar products of tensor operators \mathbf{O} and \mathbf{O}' that transform according to complex-conjugate representations Γ and Γ^* of G (because the product representation $\Gamma \times \Gamma^*$ necessarily contains Γ_1). It is preferable, though not necessary, that \mathbf{O} and \mathbf{O}' are chosen such that their representations Γ and Γ^* are irreducible under G . For the groups $D_{6h} \times C_\theta$, $O_h \times C_\theta$, and relevant subgroups discussed below, all IRs are real, $\Gamma^* = \Gamma$.

We may add terms to the Hamiltonian that describe the effect of electric and magnetic multipole densities \mathbf{m} .

The respective invariant interaction terms can be written as a sum of scalar products [52]

$$\sum_{\alpha} a_{\alpha}^G \mathbf{K}_{\alpha}^G \cdot \mathbf{m}_{\alpha}^G, \quad (6)$$

where the sum runs over the IRs Γ_{α} appearing in the decomposition (3), and the irreducible tensor operators \mathbf{K}_{α}^G transform according to the respective complex-conjugate IRs Γ_{α}^* . For brevity of notation, we ignore that, in general, we have multiple irreducible tensors \mathbf{m}_{α}^G (\mathbf{K}_{α}^G) that transform according to the same IR Γ_{α} (Γ_{α}^*) of G . Furthermore, we restrict the present analysis to effects linear in the multipole densities \mathbf{m} . The irreducible tensors \mathbf{m}_{α}^G can also be used to construct irreducible tensors of higher degree in the components of \mathbf{m} (similar to the tensor operators \mathbf{K}_{α}^G discussed below that may be higher-degree polynomials in the components of crystal momentum $\hbar\mathbf{k}$). The expansion coefficients a_{α}^G are material-specific parameters that are generally different for different electronic bands.

When the theory of invariants is applied to the dynamics of Bloch electrons, the components of the tensor operators \mathbf{K}_{α}^G are polynomials in the components of crystal momentum $\hbar\mathbf{k}$ and of spin $(\hbar/2)\boldsymbol{\sigma}$ (and sometimes also components of orbital angular momentum representing band degeneracies). Given the transformational behavior of \mathbf{k} and $\boldsymbol{\sigma}$ under G , all tensor operators \mathbf{K}_{α}^G of given degrees in \mathbf{k} and $\boldsymbol{\sigma}$ [even beyond those relevant for the decomposition (3)] can be derived in a systematic way using the coupling coefficients tabulated by Koster *et al.* [45]. This makes the theory of invariants a comprehensive theory regarding the effects induced by multipolar order on the dynamics of Bloch electrons. For systems with spherical symmetry and ignoring SIS and TIS so that the symmetry group is R , the tensor operators must transform according to the IR D_{ℓ} of the multipole density \mathbf{m} , compare Eq. (9) below. In this case, the components of the tensor operators \mathbf{K}^R can be chosen to be the familiar harmonic polynomials, the degree of which equals the order ℓ of \mathbf{m} [49]. When the symmetry group G is a finite subgroup of $R_{i \times \theta}$, the degree of the polynomials \mathbf{K}_{α}^G need not match the order ℓ of the corresponding multipole density \mathbf{m} . Instead, SIS and TIS require that the signature ss' of \mathbf{m} must equal the signature of the tensor operators \mathbf{K}_{α}^G . Therefore, the signatures

TABLE IV. Powers of cartesian components of the wave vector (collectively denoted k) and components of spin (collectively denoted σ) required for a polynomial representation of tensor operators with signature ss' associated with multipoles of order ℓ . The symbol n denotes a non-negative integer.

	electric	magnetic	electro- toroidal	magneto- toroidal
ℓ even	$+++ : k^{2n+2}$	$-- : k^{2n+1}$	$-+ : k^{2n+1}\sigma$	$+- : k^{2n}\sigma$
ℓ odd	$-+ : k^{2n+1}\sigma$	$+- : k^{2n}\sigma$	$++ : k^{2n+2}$	$-- : k^{2n+1}$

of \mathbf{k} ($--$) and $\boldsymbol{\sigma}$ ($+-$) represent constraints on the degree of the polynomials \mathbf{K}_{α}^G , see Table IV. (We do not consider higher powers in $\boldsymbol{\sigma}$ because $\sigma_j^2 = \mathbb{1}$.) For example, tensor operators \mathbf{K}_{α}^G associated with electric and magnetic multipole densities for odd ℓ necessarily involve the spin operator $(\hbar/2)\boldsymbol{\sigma}$. Purely orbital operators \mathbf{K}_{α}^G associated with odd ℓ may arise for degenerate and off-diagonally coupled bands [31, 52, 66] that are not studied in the present work. Concrete examples for how tensor operators \mathbf{K}_{α}^G represent multipoles are given in Secs. III and IV.

E. Indicators of multipolar order

We begin with the case that, for a given group G , the invariant expansion (6) is formulated for a multipole density \mathbf{m} of order $\ell < \ell_{\min}$ when $\mathbf{m} = \mathbf{0}$, and the sum over IRs Γ_{α} of G does not include the identity representation Γ_1 . In this case, the expectation values of all irreducible tensor operators \mathbf{K}_{α}^G appearing in the expansion (6) must vanish, $\langle \mathbf{K}_{\alpha}^G \rangle = \mathbf{0}$.

As discussed above, if, starting from a group G that requires $\mathbf{m} = \mathbf{0}$, the multipole density \mathbf{m} becomes nonzero (e.g., because of external perturbations or due to a phase transition), the symmetry of the system is reduced from G to a subgroup U of G , and the nonzero component m_1^U of \mathbf{m} transforms according to the identity representation Γ_1 of U . This implies, in turn, that the corresponding tensor operator K_1^U also transforms irreducibly according to Γ_1 of U and has a nonzero expectation value, $\langle K_1^U \rangle \neq 0$. The tensor operator K_1^U thus provides a probe for the presence of the multipole density m_1^U .

Given a multipole density \mathbf{m} for some ℓ , under G each irreducible component \mathbf{m}_{α}^G of \mathbf{m} defines the *indicator*

$$\mathbf{I}_{\alpha}^G = \frac{\partial H}{\partial \mathbf{m}_{\alpha}^G} = a_{\alpha}^G \mathbf{K}_{\alpha}^G \quad (7)$$

as an operator that is independent of the presence of the multipole density \mathbf{m} . In a system without multipolar order, i.e., when the group G requires $\mathbf{m} = \mathbf{0}$, the expectation value $\langle \mathbf{I}_{\alpha}^G \rangle$ must vanish, $\langle \mathbf{I}_{\alpha}^G \rangle = \mathbf{0}$ because $\Gamma_{\alpha} \neq \Gamma_1$. Conversely, when some component m_1^U of \mathbf{m}_{α}^G becomes finite, the respective component $\langle I_1^U \rangle$ of $\langle \mathbf{I}_{\alpha}^G \rangle$ becomes nonzero. For small $|\mathbf{m}_{\alpha}^G|$, the expectation value $\langle \mathbf{I}_{\alpha}^G \rangle$ is given by the linear-response expression

$$\langle \mathbf{I}_{\alpha}^G \rangle = \chi_{\alpha}^G \mathbf{m}_{\alpha}^G, \quad (8)$$

with the matrix χ_{α}^G denoting the static uniform \mathbf{I}_{α}^G - \mathbf{I}_{α}^G response function [67] in the parent structure with group G . According to Eq. (8), the expectation value $\langle \mathbf{I}_{\alpha}^G \rangle$ is a direct quantitative probe of the multipole density \mathbf{m} . Therefore, in the system with point group U , where the nonzero component of $\langle \mathbf{I}_{\alpha}^G \rangle$ is given by $\langle I_1^U \rangle$, we have $m_1^U = [\chi_{\alpha}^G]^{-1} \langle I_1^U \rangle$.

A familiar example for the indicator formalism is given by exchange coupling in ferromagnets. Here the invariant is an exchange term $(g/2)\mu_B \boldsymbol{\sigma} \cdot \boldsymbol{x}$ with magnetic dipole density \boldsymbol{x} . The g -factor g is generally an effective parameter that characterizes the parent structure with group G ; it may deviate from the free-electron value $g = 2$ [68, 69]. In an anisotropic crystal environment, the exchange term may break up into multiple invariant terms representing different crystallographic directions and weighted with different g -factors g [52]. The indicator representing exchange coupling is the magnetic-moment operator $(g/2)\mu_B \boldsymbol{\sigma}$ whose nonzero expectation value signals the presence of ferromagnetic order. After the system has undergone a phase transition to a ferromagnetic state, the nonzero component of $\langle (g/2)\mu_B \boldsymbol{\sigma} \rangle$ is given by $\chi_P^G \boldsymbol{x}_1^U$, with χ_P^G denoting the Pauli susceptibility in the parent structure. Knowing the latter thus enables determination of the ferromagnetic structure's magnetic dipole density via $\boldsymbol{x}_1^U = [\chi_P^G]^{-1} \langle (g/2)\mu_B \boldsymbol{\sigma} \rangle$.

For a structure with group U giving $\boldsymbol{m}_1^U \neq 0$, the parent structure with group $G \supseteq U$ and $\boldsymbol{m} = 0$ takes the role of a reference state. The need for a reference state also arises in the modern theories of electric dipolarization [4, 70] and orbital magnetization [71, 72] that do not define these quantities on an absolute scale. Instead, they are defined as differences between two states of the material that can be connected by an adiabatic switching process [2, 5]. Similarly, it was noticed in an early study of the thermodynamics of pyroelectricity that only the differences between the dipolarization in different states of the system are physically significant [7].

F. Symmetry hierarchies

The irreducible components \boldsymbol{m}_α^G and \boldsymbol{m}_β^U of electric and magnetic multipole densities \boldsymbol{m} of different order ℓ that are permitted by different crystallographic groups G and subgroups U define a physically motivated hierarchy among these groups. This hierarchy is complemented by a matching hierarchy of tensor operators \mathbf{K}_α^G and \mathbf{K}_β^U that obey the same sequence of compatibility relations (for the complex conjugate IRs) as \boldsymbol{m}_α^G , and \boldsymbol{m}_β^U [Eqs. (3) and (5)].

The hierarchy can be extended to include the rotation group $R_{i \times \theta}$ at the top, known as spherical approximation to the dynamics of Bloch electrons [31, 73]. Under $R_{i \times \theta}$, the invariant interaction between a spherical multipole density \boldsymbol{m} and crystal electrons can be written as a scalar product [49] similar to Eq. (6)

$$a^R \mathbf{K}^R \cdot \boldsymbol{m}. \quad (9)$$

Here, conceptually similar to the tensor operators \mathbf{K}_α^G , the components of \mathbf{K}^R are harmonic polynomials in the components of crystal momentum $\hbar \mathbf{k}$ and spin $(\hbar/2)\boldsymbol{\sigma}$. Ignoring SIS and TIS, the harmonic polynomials transforming according to the IR D_ℓ of R can be chosen as

polynomials of degree ℓ [49]. With SIS and TIS taken into account, the polynomials \mathbf{K}^R must transform according to the IR $D_\ell^{ss'}$ of $R_{i \times \theta}$ so that these polynomials are at least of degree ℓ to be consistent with Table IV. By definition, an electric monopole density $\ell = 0$ transforms according to the identity representation D_0^{++} of $R_{i \times \theta}$, i.e., it is always allowed in the spherical approximation. The corresponding scalar tensor operators K^R are given by even powers of the wave vector \mathbf{k} .

Often in applications of the theory of invariants to the dynamics of Bloch electrons, the main physics is already captured by a Hamiltonian H with spherical symmetry, i.e., a Hamiltonian that is invariant under the rotation group $R_{i \times \theta}$ [31, 73]. Starting from such a model we can add successively the effect of electric and magnetic multipoles \boldsymbol{m} of decreasing order ℓ till the symmetry is reduced to the actual symmetry group G_0 of the real system. (This concept has been called *symmetry hierarchy* [31] or *hierarchy of approximations* [74]. Conceptually, this approach is closely related to the virtual crystal approximation employed in first-principles electronic band-structure methods [75].) The importance of different multipoles \boldsymbol{m} is reflected by the magnitude of the prefactors a^G appearing in the invariant expansion for these multipoles. Commonly, the magnitude of the prefactors a^G decreases with decreasing order ℓ of the multipoles [31, 73, 74, 76].

Interestingly, this well-established scheme appears to violate the fact known for finite localized systems that only the multipole \boldsymbol{M} of lowest nonvanishing order $\ell = \ell_{\min}$ is well-defined because the coefficients of the higher-order multipoles \boldsymbol{M} depend in general on the choice of origin [34, 35]. However, the situation is qualitatively different in extended crystalline solids where even the multipole density \boldsymbol{m} of lowest nonvanishing order $\ell = \ell_{\min}$ cannot be defined in terms of multipole moments per unit cell because this multipole moment depends on the arbitrary definition of a unit cell [3]. The modern theory of electric dipolarization and magnetization thus defines the $\ell = 1$ multipole densities in terms of geometric phases that are independent of the definition of the unit cell [1, 2].

In crystalline solids, the non-uniqueness of higher-order multipoles takes a distinct twist. Within each family of polarizations (even- ℓ electric, odd- ℓ electric, even- ℓ magnetic, and odd- ℓ magnetic), the respective invariants appearing in the expansion (6) are not uniquely defined, as any linear combination of invariants in a family is again an invariant in that family, see footnote 35 in Ref. [76]. For a crystal structure with symmetry group G_0 , this ambiguity is resolved, but only for the multipole density \boldsymbol{m} of lowest nonvanishing order in each family, by requiring that the tensor operator $K_1^{G_0}$ associated with $\boldsymbol{m}_1^{G_0}$ has a vanishing projection on the identity representation Γ_1 of the supergroup $G \supseteq G_0$ that characterizes the system when $\boldsymbol{m} = \mathbf{0}$. This implies that even- ℓ electric (magnetic) multipole densities can be defined (together with their associated invariants) independent of

odd- ℓ electric (magnetic) multipole densities.

For example, pristine diamond with point group O_h supports an electric hexadecapole density $\ell = 4$, see Sec. IV A. If the symmetry is reduced from $O_h = O \times C_i$ to O , the system also supports electric multipole densities with odd ℓ . However, the lowest-order electric multipole density with odd ℓ permitted by the group O has $\ell = 9$ (while the associated lowest-degree invariant is of Dirac type, $a^{(e,9)}\mathbf{m}^{(e,9)} \cdot \boldsymbol{\sigma} \cdot \mathbf{k}$, see Sec. V, i.e., it corresponds to $n = 0$ in the notation of Table IV). For a system with point group O , the electropolarization with $\ell = 9$ and its associated invariant are well-defined, despite the concurrent presence of a parapolarization with $\ell = 4$ (hexadecapolarization).

G. Band-dispersion characteristics of the categories of polarized matter

According to Table IV, the five categories of polarized matter have unique patterns of band dispersions $E_\sigma(\mathbf{k})$ as sketched in Fig. 1. Band degeneracies for the five categories are summarized in Table V. The parapolar category with the highest symmetry is characterized by a spin-degenerate band dispersion that only involves even powers of the wave vector \mathbf{k} . The patterns exhibited by the remaining four categories depend on the non-negative integer n determining the powers of the cartesian components of the wave vector \mathbf{k} ; see Table IV. Generally, the case $n = 0$ is qualitatively distinct from $n \geq 1$. When $n = 0$ (lower row in Fig. 1) the electropolar, the antimagnetopolar and the multipolar categories are characterized via a finite slope of the dispersion at $k = 0$.

More specifically, the patterns of band dispersions depend on the particular tensor operators that couple to the multipole densities \mathbf{m} according to the theory of invariants. This is illustrated in Table VI for the invariants associated with multipole densities in the diamond family. (These invariants are derived in Sec. IV.) The electropolar category with $n = 0$ is realized by Rashba spin-orbit coupling [28], while the case $n = 1$ includes Dresselhaus spin-orbit coupling [33]. The magnetopolar category with $n = 0$ yields the exchange coupling in ferromagnets, while for $n = 1$ it includes altermagnets [77–79]. An example for the antimagnetopolar category

TABLE V. Band degeneracies imposed by inversion symmetries for the categories of polarized matter. Lines connect band energies that are equal.

category		$E_\sigma(\mathbf{k})$	$E_\sigma(-\mathbf{k})$	$E_{\bar{\sigma}}(\mathbf{k})$	$E_{\bar{\sigma}}(-\mathbf{k})$
parapolar	$C_{i \times \theta}$	•	•	•	•
electropolar	C_θ	•	•	•	•
magnetopolar	C_i	•	•	•	•
antimagnetopolar	$C_{i\theta}$	•	•	•	•
multipolar	C_1	•	•	•	•

with $n = 1$ is the Néel term in diamond antiferromagnets derived in Ref. [66].

H. Toroidal moments

For each $\ell = 0, 1, 2, \dots$ the rotation group $R_{i \times \theta}$ has four IRs $D_\ell^{ss'}$. As discussed in Sec. II A, for even ℓ , electric (magnetic) multipole densities transform according to D_ℓ^{++} (D_ℓ^{--}), while for odd ℓ , electric (magnetic) multipole densities transform according to D_ℓ^{-+} (D_ℓ^{+-}). The remaining IRs for each ℓ have been associated with electrotoroidal ($D_\ell^{\mp+}$) and magnetotoroidal ($D_\ell^{\pm-}$) moments [39–43], see Table I. However, the physical significance of toroidal moments has recently been questioned [44].

It was suggested that toroidal moments can be observed in (magnetic) crystalline environments [39–41] when these moments become symmetry-allowed, similar to the electric and magnetic multipole densities discussed above [80]. However, unlike the rotation group $R_{i \times \theta}$, each of the (magnetic) crystallographic point groups G possesses only a finite set $\{\Gamma_\alpha\}$ of IRs so that under symmetry reduction $R_{i \times \theta} \mapsto G$, the toroidal moments are mapped onto the same set $\{\Gamma_\alpha\}$ as the electric and magnetic moments [45]. According to Table II, each family of electromagnetic multipoles with even (odd) ℓ has a matching family of toroidal moments with odd (even) ℓ , but the same signature ss' . These pairs of families thus have the same transformational behavior under SIS and TIS and they couple to the same indicators (Table IV). Therefore, under the smaller groups G , toroidal moments represent the same observable physics as electric and magnetic moments. Below, we illustrate this point for crystal structures that are members of the lonsdaleite and diamond families. Toroidal moments are fundamentally distinct from electromagnetic multipoles only under the rotation group $R_{i \times \theta}$, but not under finite subgroups of $R_{i \times \theta}$.

Similar to electric and magnetic multipole densities \mathbf{m} , for each crystallographic group G we can identify the lowest-order electrotoroidal ($\ell_{\min}^{(et,\lambda)}$) and magnetotoroidal ($\ell_{\min}^{(mt,\lambda)}$) moments that are permitted by symmetry. Generally there is no simple relation between, on the one hand, $\ell_{\min}^{(e,\lambda)}$ and $\ell_{\min}^{(m,\lambda)}$, and, on the other hand, $\ell_{\min}^{(et,\bar{\lambda})}$ and $\ell_{\min}^{(mt,\bar{\lambda})}$, where $\bar{\lambda} = u$ ($\bar{\lambda} = g$) for $\lambda = g$ ($\lambda = u$). For example, the point group D_{6h} of lonsdaleite permits an electric quadrupole density ($\ell = 2$), whereas the lowest electrotoroidal multipole permitted by D_{6h} has $\ell = 7$. Conversely, the lowest order of a magnetic multipole density permitted by the group $D_{6h}(C_{6v})$ has $\ell = 6$ whereas the same group permits a magnetotoroidal multipole with $\ell = 1$. This is similar to the fact discussed above that, under crystallographic point groups G , the order ℓ of a multipole density \mathbf{m} need not equal the polynomial degree of the tensor operators \mathbf{K}_α^G associated with \mathbf{m} in the invariant expansion (6).

TABLE VI. Invariants associated with multipolar order in the diamond family. Here $\mathbf{m}^{(e,\ell)}$ and $\mathbf{m}^{(m,\ell)}$ denote the order- ℓ electric and magnetic multipole densities considered in Sec. IV, and n is the non-negative integer defined in Table IV.

ss'	$n = 0$	$n = 1$	$n > 1$
++	$m_x^{(e,2)} (-2k_x^2 + k_y^2 + k_z^2) + \text{cp}^a$	$m^{(e,4)} (k_x^2 k_y^2 + \text{cp})$	
-+	$m_x^{(e,1)} (\sigma_y k_z - \sigma_z k_y) + \text{cp}^a$	$m^{(e,3)} [\sigma_x k_x (k_y^2 - k_z^2) + \text{cp}]$	
+-	$m_x^{(m,1)} \sigma_x + \text{cp}$	$m^{(m,3)} (\sigma_x k_y k_z + \text{cp})$	
--	$m_x^{(m,2)} k_x + \text{cp}^b$	$m_x^{(m,2)} k_x (k_y^2 - k_z^2) + \text{cp}$	$m^{(m,4)} k_x k_y k_z (k_y^2 - k_z^2) (k_z^2 - k_x^2) (k_x^2 - k_y^2)$

^a Realized in strained or quantum-confined diamond.

^b Realized in strained or quantum-confined diamond antiferromagnets.

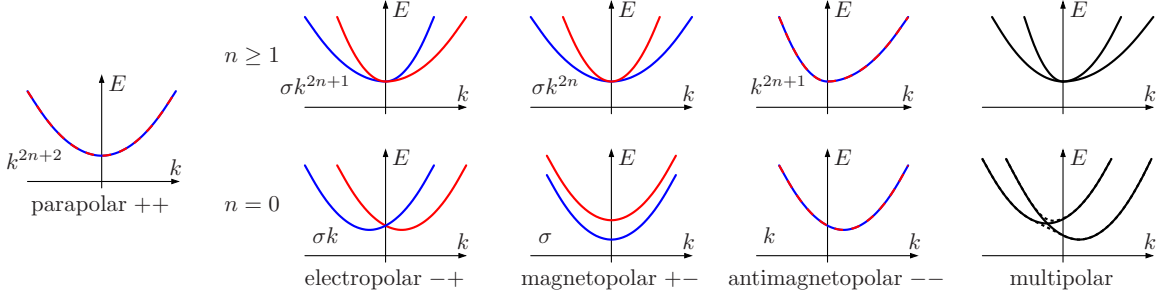


FIG. 1. Typical examples for spinful band dispersions $E_\sigma(\mathbf{k})$ associated with the five categories of polarized matter. The bands for the parapolar and antimagnetopolar categories are at least twofold spin-degenerate in the entire Brillouin zone. The upper (lower) row corresponds to $n \geq 1$ ($n = 0$), where n is defined in Table IV. The expressions in the lower left of the panels use the simplified notation of Table IV to represent the indicators for the presence of multipolar order. Different colors represent opposite spin orientations. In the multipolar case, the spin-split bands have more complicated spin textures such that it is generally not possible to assign a spin index to these bands.

I. Macroscopic multipole densities and localized multipoles

According to Neumann's principle, the pattern of macroscopic multipole densities \mathbf{m} permitted in a crystal structure is determined by the crystallographic point group G defining the crystal class of the crystal structure [7, 8, 52]. For crystal structures transforming according to a symmorphic space groups S , the point group G is the finite subgroup of S consisting of the elements of S that leave one point in space fixed. Nonsymmorphic space groups S also contain group elements that combine point group symmetries g with nonprimitive translations. Here the elements g are also elements of the point group G , although these symmetry operations are not, by themselves, elements of S . The latter case makes crystallographic point groups defining crystal classes qualitatively distinct from point group symmetries of finite systems like molecules.

The macroscopic multipole densities \mathbf{m} can be realized microscopically by localized multipoles \mathcal{M} that are arranged periodically consistent with the space group S . The length scale of the localized multipoles \mathcal{M} is generally a fraction of the lattice constant. The permitted patterns of multipoles \mathcal{M} are determined by the site symmetries characterizing the Wyckoff positions of the atoms forming a crystal structure. The site symmetries

are subgroups of the crystallographic point group G ; this is the reason why the order of the multipoles \mathcal{M} may be smaller (or larger) than the order of the resulting multipole density \mathbf{m} . Generally, there is no simple relation between the order of local multipoles \mathcal{M} and the order of the resulting macroscopic multipole density \mathbf{m} . The site symmetries are tabulated in Refs. [37, 38], see also Refs. [81, 82].

For example, the site symmetry of the atoms in the lonsdaleite structure discussed below is the group C_{3v} that permits a local electric dipole moment, but also an electric octupole moment [45]. The latter is realized by the sp^3 hybrid orbitals with which elements like carbon form lonsdaleite. A TB picture is well-suited to discuss the local electronic structure of the atoms as a function of their positions in a crystal structure, see Ref. [83] for a more detailed analysis. The concept of site symmetries and the localized multipoles permitted by these site symmetries is independent of the ambiguous definition of a unit cell for a crystal structure [3].

For magnetic structures, it is well-known that local magnetic dipole moments on the atoms affect their site symmetries [84]. These constraints determine the magnetic space groups of these structures and thus, in turn, also the magnetic point group G . We extend this scheme by also considering local magnetic multipoles of higher order beyond $\ell = 1$ [36]. Throughout we consider macro-

scopic electric and magnetic multipole densities on the same footing. Likewise, we consider local electric and magnetic multipoles on the same footing. The local multipoles \mathcal{M} attached to atomic sites in a crystal provide an instructive physical picture for the microscopic origin of the macroscopic multipole densities \mathbf{m} . Also, magnetic multipoles \mathcal{M} attached to atomic sites provide a convenient means to incorporate magnetic order into TB models. For conceptual clarity, we limit our discussion of examples in Secs. III and IV to configurations with local multipoles \mathcal{M} of only one order ℓ , even though computational studies of real materials typically observe a greater variety of such multipoles [85].

III. LONSDALEITE FAMILY

As an illustration for how to apply the general theory developed in Sec. II, we analyze electric and magnetic order in variants of hexagonal lonsdaleite listed in Table III. In Sec. III A, we consider the electric quadrupolarization that is already present in pristine lonsdaleite and therefore exists alongside all other polarizations that reduce the high symmetry of the lonsdaleite crystal structure. We then discuss electropolarizations in Secs. III B (electric octupolarization) and III C (electric dipolarization). Magnetopolarizations are covered in Secs. III E (magnetic octupolarization) and III G (magnetization), while results for antimagnetopolarizations are presented in Secs. III D (magnetic hexadecapolarization) and III F (magnetic quadrupolarization). Section III H is devoted to an elucidation of close connections between electric and magnetic orders.

To simplify the presentation, we always ignore TIS when analyzing electric order. As explained in Sec. II C, we identify IRs of magnetic point groups by referring to the respective nonmagnetic subgroups as tabulated by Koster *et al.* [45]; and we indicate the homomorphisms relating the magnetic groups with their nonmagnetic subgroups via an arrow ‘ \rightarrow ’. Within each subsection, we follow the same outline. We start by discussing the crystal symmetry and stating the compatibility relations for the relevant multipole density. We then identify the terms in the Bloch-electron Hamiltonian linear in the considered multipole density having lowest order in \mathbf{k} and discuss associated physical ramifications. Then we link the local site symmetry with its allowed local multipoles to the bulk multipole density. We also identify the toroidal moment density that manifests itself via the same invariants as the discussed electric or magnetic multipole density.

A. Electric quadrupolarization in pristine lonsdaleite

The hexagonal nonsymmorphic lonsdaleite structure is shown in Fig. 2(c). The space group of lonsdaleite is D_{6h}^4 (No. 194, $P6_3/mmc$). Ignoring TIS, the crystallo-

graphic point group of lonsdaleite is $D_{6h} = D_6 \times C_i$, i.e., lonsdaleite is parapar. The lowest nonvanishing electric multipole density allowed by D_{6h} is an electric quadrupolarization ($\ell = 2$) with compatibility relation [45]

$$R_i \mapsto D_{6h} : D_2^+ \mapsto \Gamma_1^+ + \Gamma_5^+ + \Gamma_6^+. \quad (10)$$

Specifically, it is the component $m = 0$ of the IR D_2^+ of R_i that transforms according to Γ_1^+ of D_{6h} when the symmetry is reduced from R_i to D_{6h} . Thus, written in cartesian coordinates, the traceless electric quadrupole density in lonsdaleite has nonzero components [34, 49]

$$\mathbf{m}^{(e,2)} \equiv m_{xx}^{(e,2)} = m_{yy}^{(e,2)} = -\frac{1}{2} m_{zz}^{(e,2)}. \quad (11)$$

Here $m^{(e,2)}$ is the scalar of the electric quadrupole density under D_{6h} . Accordingly, the harmonic polynomial in the components of \mathbf{k} for $\ell = 2$ and $m = 0$

$$K_1^{(e,2)} = k_x^2 + k_y^2 - 2k_z^2 \quad (12)$$

yields the invariant

$$\begin{aligned} H^{(e,2)} &= a^{(e,2)} \mathbf{m}^{(e,2)} K_1^{(e,2)} \\ &= a^{(e,2)} \mathbf{m}^{(e,2)} (k_x^2 + k_y^2 - 2k_z^2), \end{aligned} \quad (13)$$

that represents an effective-mass anisotropy in the energy dispersion $E_\sigma(\mathbf{k})$ of band electrons in lonsdaleite [86]. The indicator $I_1^{(e,2)} = a^{(e,2)} K_1^{(e,2)}$ thus signals the electric quadrupole density in lonsdaleite [87].

The site symmetry of the atoms forming the lonsdaleite structure is the group C_{3v} [37] that permits a local electric dipole moment oriented along the main axis of lonsdaleite [45]. The group C_{3v} also permits an electric octupole moment that is naturally realized by the sp^3 hybrid orbitals with which elements like carbon form lonsdaleite [Fig. 2(g)], analogous to the electric octupole moment of tetrahedrally bonded molecules such as CH_4 [88]. It is the microscopic octupole that creates the bulk quadrupolarization. The electric quadrupolarization (11) in pristine lonsdaleite and the associated invariant (13) are also present in all other members of the lonsdaleite family discussed in the remainder of this section. In that sense, the presence of the electric quadrupolarization (11) represents a key feature of the lonsdaleite family.

The lowest electrotoroidal moment permitted in pristine lonsdaleite has $\ell = 7$. It manifests itself via the same invariant (13) as the electric quadrupole density.

B. Electric octupolarization in lonsdaleite

Pristine lonsdaleite has four identical atoms per unit cell [Fig. 2(c)], and its lowest-order multipole density is a quadrupolarization (Sec. III A). Two distinct types of atoms arranged as in Fig. 2(b) reduce the space-group symmetry to D_{3h}^1 (No. 187, $P6m2$) and the point-group symmetry is reduced to D_{3h} . The group D_{3h} breaks SIS

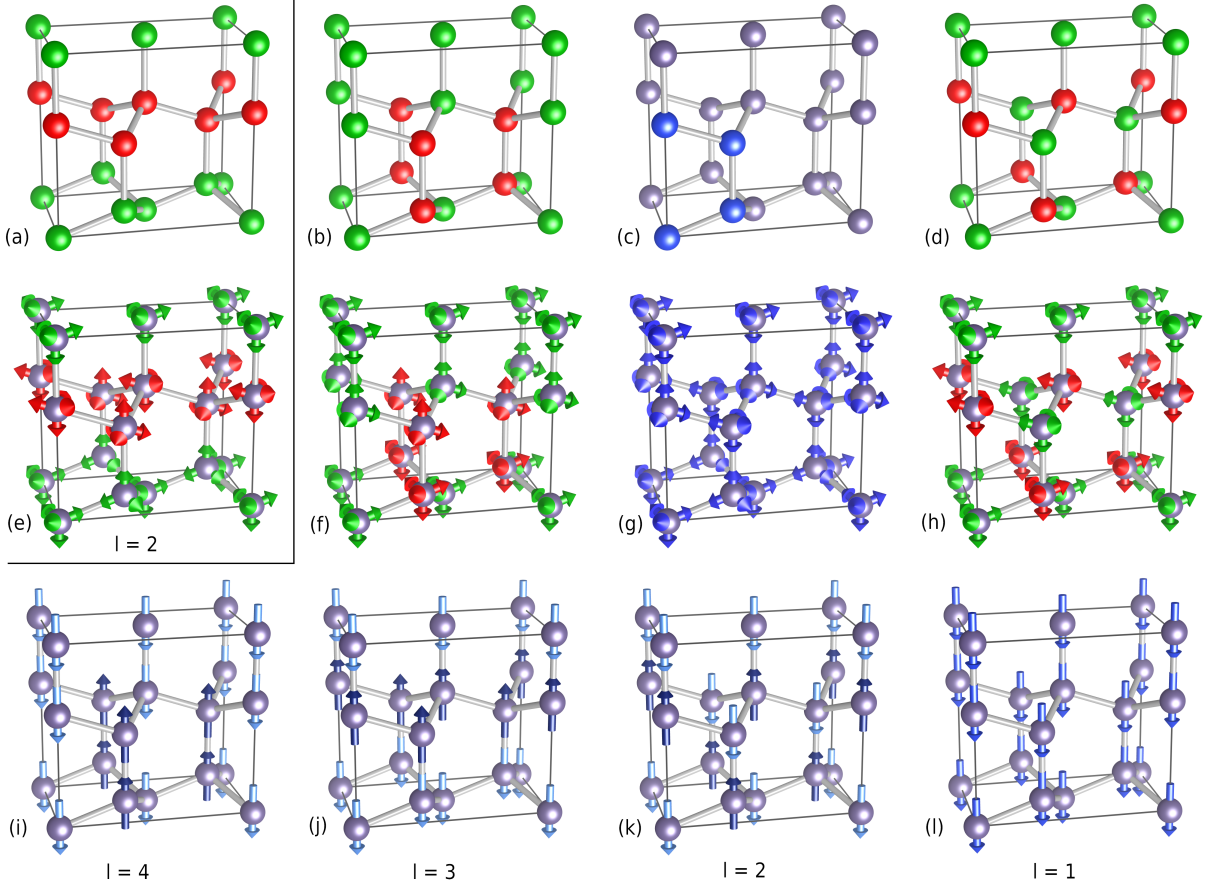


FIG. 2. Multipole densities in the lonsdaleite family. Top row [(a), (b), (c), and (d)]: pristine lonsdaleite (c) and variants of the lonsdaleite crystal structure including wurtzite (d). In (c), the four atoms in a unit cell are highlighted in blue. (g) The local electric octupole moments \mathcal{M}_0 on the identical atoms in pristine lonsdaleite give rise to an electric quadrupolarization ($\ell = 2$). Remaining panels in the central row [(e), (f), and (h)]: For the structures (a), (b), and (d) consisting of two distinct types of atoms, panels (e), (f), and (h) show the deviation $\Delta\mathcal{M}$ of the local octupole moments compared with the moments \mathcal{M}_0 when all atoms are identical [panel (g)]. These local moments $\Delta\mathcal{M}$ give rise to (e) an electric quadrupolarization ($\ell = 2$), (f) an octupolarization ($\ell = 3$), and (h) a dipolarization ($\ell = 1$). Bottom row [(i), (j), (k), and (l)]: local magnetic dipole moments give rise to (i) a hexadecapolarization ($\ell = 4$), (j) an octupolarization ($\ell = 3$), (k) a quadrupolarization ($\ell = 2$), and (l) a magnetization ($\ell = 1$). Panels (i), (j), (k), and (l) show the local magnetic dipole moments with different shades of the same color because all sites are equivalent by symmetry (i.e., they have the same Wyckoff letter) so that the local moments are likewise symmetry-equivalent. The same situation arises for the electric octupole moments (g) of the nonmagnetic pristine lonsdaleite structure (c).

so that this structure is electropolar. The lowest-order electric multipole density supported by the crystal structure in Fig. 2(b) is an electric octupole density ($\ell = 3$) that yields the compatibility relation [45]

$$R_i \mapsto D_{3h} : \quad D_3^- \mapsto \Gamma_1 + \Gamma_2 + \Gamma_4 + \Gamma_5 + \Gamma_6. \quad (14)$$

The corresponding invariants in the Hamiltonian read (to lowest order in \mathbf{k})

$$H^{(e,3)} = a^{(e,3)} m^{(e,3)} k_z \left[\sigma_x k_x k_y + \frac{1}{2} \sigma_y (k_x^2 - k_y^2) \right] + b^{(e,3)} m^{(e,3)} \sigma_z k_y (3k_x^2 - k_y^2). \quad (15)$$

These terms represent a spin-orbit coupling.

The site symmetry of the atoms is, once again, C_{3v} [37]. However, the two distinct atoms in Fig. 2(b)

have different Wyckoff positions (with two atoms of each type per unit cell), and they may carry different electric octupole moments. We decompose these moments $\mathcal{M} \equiv \mathcal{M}_0 + \Delta\mathcal{M}$ into one part \mathcal{M}_0 that is equal by symmetry for all atoms as in lonsdaleite. These moments thus have the same observable effect as the local moments in pristine lonsdaleite [Fig. 2(g)], i.e., they give rise to the invariant (13). It is the remaining part $\Delta\mathcal{M}$ oriented oppositely that is shown in Fig. 2(f) and that gives rise to the new invariants (15). This can be worked out quantitatively in a simple sp^3 TB model [89].

The lowest electrotoroidal moment permitted in this structure has $\ell = 4$.

C. Electric dipolarization in lonsdaleite – wurtzite

If two of the four identical atoms in the lonsdaleite unit cell become distinct as shown in Fig. 2(d), we obtain the wurtzite structure that is realized by several III-V and II-VI semiconductors including ZnS, CdSe, GaN, and AlN. The space group becomes C_{6v}^4 (No. 186, $P6_3mc$), and the point group of wurtzite is C_{6v} . These groups break SIS so that wurtzite is electropolar. More specifically, the compatibility relation [45]

$$R_i \mapsto C_{6v} : D_1^- \mapsto \Gamma_1 + \Gamma_5 \quad (16)$$

indicates that wurtzite naturally permits an electric dipole density ($\ell = 1$, an electric dipolarization). The associated invariant in the Hamiltonian to lowest order in \mathbf{k} ,

$$H^{(e,1)} = a^{(e,1)} m^{(e,1)} (\sigma_x k_y - \sigma_y k_x) , \quad (17)$$

represents a spin-orbit coupling commonly known as Rashba term [28].

A more complete analysis of the electric dipole density in wurtzite is given in Table VII. Ignoring TIS, the dipole density transforms according to D_1^- of R_i . A hexagonal environment (point group D_{6h}) yields the compatibility relation [45]

$$R_i \mapsto D_{6h} : D_1^- \mapsto \Gamma_2^- + \Gamma_5^- , \quad (18)$$

so that, as to be expected, a dipole density is forbidden in lonsdaleite. The lowest-order tensor operator transforming like Γ_2^- is

$$K_{2-}^{(e,1)} = \sigma_x k_y - \sigma_y k_x , \quad (19)$$

while two pairs of operators transform like Γ_5^-

$$K_{5-}^{(e,1)} : \sigma_y k_z, -\sigma_x k_z; \sigma_z k_y, -\sigma_z k_x . \quad (20)$$

The expectation value of these operators must thus vanish in lonsdaleite. When the symmetry is further reduced to C_{6v} (wurtzite), we get the compatibility relations [45]

$$D_{6h} \mapsto C_{6v} : \begin{cases} \Gamma_2^- \mapsto \Gamma_1, & \Gamma_5^- \mapsto \Gamma_5 \\ K_{2-}^{(e,1)} \mapsto K_1^{(e,1)}, & K_{5-}^{(e,1)} \mapsto K_5^{(e,1)} , \end{cases} \quad (21)$$

so that the tensor operator (19) becomes allowed and yields the Rashba term (17).

Just as in Sec. III B, the distinct atoms in wurtzite have different Wyckoff positions, but they all have the site symmetry C_{3v} [37]. The local electric moments on the atoms are illustrated in Fig. 2(h).

The lowest electrotoroidal moment permitted in wurtzite has $\ell = 6$.

D. Magnetic hexadecapolarization in lonsdaleite

If the four equivalent atoms in the lonsdaleite unit cell carry magnetic dipole moments as in Fig. 2(i), the system

TABLE VII. Irreducible representations (IRs) and their lowest-order representative basis functions of an electric dipole (signature $-+$) and magnetic dipole (signature $+ -$) oriented along the main axis of a hexagonal crystalline environment. The IRs are labeled according to Koster *et al.* [45].

$R_{i \times \theta} \rightarrow R_i$	$D_1^{-+} \rightarrow D_1^-$	
$D_{6h} \times C_\theta \rightarrow D_{6h}$	Γ_2^- $\sigma_x k_y - \sigma_y k_x$	$+$ Γ_5^- $\sigma_y k_z, -\sigma_x k_z;$ $\sigma_z k_y, -\sigma_z k_x$
$C_{6v} \times C_\theta \rightarrow C_{6v}$	Γ_1	Γ_5
$R_{i \times \theta} \rightarrow R_i$	$D_1^{+-} \rightarrow D_1^+$	
$D_{6h} \times C_\theta \rightarrow D_{6h}$	Γ_2^+ σ_z	$+$ Γ_5^+ σ_x, σ_y
$D_{6h}(C_{6h}) \rightarrow C_{6h}$	Γ_1^+	$\Gamma_5^+ + \Gamma_6^+$

becomes antimagnetopolar. More specifically, the magnetic space group becomes $P6'_3/m'm'c$ (No. 194.266) and the magnetic point group becomes $D_{6h}(D_{3h}) \rightarrow D_{3h}$ that supports in lowest order a magnetic hexadecapole density ($\ell = 4$) for which the compatibility relation reads

$$R_i \mapsto D_{3h} : D_4^- \mapsto \Gamma_1 + \Gamma_2 + \Gamma_3 + 2\Gamma_5 + \Gamma_6 . \quad (22)$$

The corresponding invariant in the Hamiltonian reads (to lowest order in \mathbf{k})

$$H^{(m,4)} = a^{(m,4)} m^{(m,4)} k_x (k_x^2 - 3k_y^2) . \quad (23)$$

The atoms with magnetic dipole moment aligned along the lonsdaleite main axis have the site symmetry $C_{3v}(C_3)$. The same site symmetry is also realized in the magnetized versions of lonsdaleite discussed in the remainder of this section. In an sp^3 TB model [89] the magnetic dipoles can be implemented via a local Zeeman term.

E. Magnetic octupolarization in lonsdaleite

If the four equivalent atoms in the lonsdaleite unit cell carry magnetic dipole moments as in Fig. 2(j), the system becomes magnetopolar. More specifically, the magnetic space group becomes $P6'_3/m'm'c$ (No. 194.268) and the magnetic point group becomes $D_{6h}(D_{3d}) \rightarrow D_{3d}$ that supports in lowest order a magnetic octupole density ($\ell = 3$) for which the compatibility relation reads

$$R_i \mapsto D_{3d} : D_3^+ \mapsto \Gamma_1^+ + 2\Gamma_2^+ + 2\Gamma_3^+ . \quad (24)$$

The corresponding invariant in the Hamiltonian reads (to lowest order in \mathbf{k})

$$H_1^{(m,3)} = a^{(m,3)} m^{(m,3)} \sigma_z k_x k_z (k_x^2 - 3k_y^2) . \quad (25)$$

Such a spin-splitting term induced by exchange coupling and proportional to an even power of components of \mathbf{k} has

recently been associated with altermagnetism [78, 79]. This term aligns the magnetic moments of the Bloch electrons (anti-)parallel to the local magnetic moments on the individual atoms [Fig. 2(j)]. The combined effect of nonrelativistic exchange coupling and relativistic spin-orbit coupling gives rise to additional invariants

$$H_2^{(m,3)} = b^{(m,3)} \mathbf{m}^{(m,3)} (\sigma_x k_y - \sigma_y k_x) k_z + c^{(m,3)} \mathbf{m}^{(m,3)} \left[\frac{1}{2} \sigma_x (k_y^2 - k_x^2) + \sigma_y k_x k_y \right], \quad (26)$$

which are also proportional to $\mathbf{m}^{(m,3)}$ and an even power of components of \mathbf{k} . These terms are typically smaller in magnitude than the nonrelativistic term (25) and tend to align the magnetic moments of the Bloch electrons perpendicular to the local magnetic moments on the individual atoms.

A momentum-dependent spin splitting of the form $\sigma_z k_x k_y$ has recently been found in MnF_2 [90], where it was called ‘‘AFM-induced spin splitting’’. See also Ref. [77]. MnF_2 has a tetragonal rutile structure. Its magnetic point group is $D_{4h}(D_{2h}) = D_4(D_2) \times C_i$ [91], making the system magnetopolar. Similar to the hexagonal magnetic structure discussed here, the tetragonal point group $D_{4h}(D_{2h})$ of MnF_2 has $\ell_{\min}^{(m)} = 3$, i.e., the lowest allowed magnetic multipole density is an octupole [18]. While Refs. [77, 90] focused on magnetic space groups to discuss the AFM-induced spin splitting, magnetic point groups are sufficient to discuss this effect [8, 52, 91]. Among the candidate materials proposed to exhibit altermagnetism [79], CrSb has the same space group and thus also the same point group $D_{6h}(D_{3d})$ as the magnetically ordered structure depicted in Fig. 2(j) and, therefore should exhibit all of the properties discussed above.

F. Magnetic quadrupolarization in lonsdaleite

A magnetic quadrupole density in lonsdaleite is analyzed in Table VIII. When going from the rotation group $R_{i \times \theta} \rightarrow R_i$ to $D_{6h} \times C_\theta \rightarrow D_{6h}$, the compatibility relation for a magnetic quadrupole $D_2^- \rightarrow D_2^-$ reads

$$R_i \mapsto D_{6h} : D_2^- \mapsto \Gamma_1^- + \Gamma_5^- + \Gamma_6^-, \quad (27)$$

so that the quadrupole remains forbidden. The lowest-order tensor operators transforming according to the IRs Γ_1^- , Γ_5^- , and Γ_6^- and consistent with the signature $--$ of a magnetic quadrupole density are listed in Table VIII.

If the four equivalent atoms in the unit cell of lonsdaleite possess oppositely oriented local magnetic moments pointing parallel to the lonsdaleite main axis [Fig. 2(k)], the system acquires a magnetic quadrupole density that yields the magnetic space group $P6_3/m'm'c'$ (No. 194.271), and the point group symmetry is reduced from $D_{6h} \times C_\theta = D_6 \times C_{i \times \theta}$ to $D_{6h}(D_6) = D_6 \times C_{i\theta}$. The system is thus antimagnetopolar. More specifically, it is the $m = 0$ component of the quadrupole density

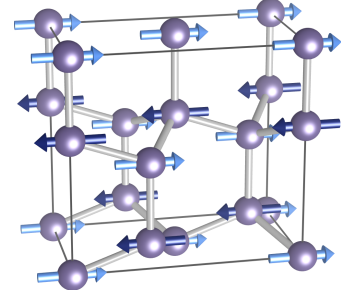


FIG. 3. Magnetic lonsdaleite with oppositely oriented local magnetic moments pointing perpendicular to the lonsdaleite main axis, compare Fig 2(k). The local moments give rise to a magnetic quadrupolarization ($\ell = 2$).

that becomes nonzero and transforms according to Γ_1 of $D_{6h}(D_6)$. The compatibility relations and lowest-order tensor operators for these IRs are listed in Table VIII. Under $D_{6h}(D_6)$, magnetic order is then signaled by a nonzero expectation value of

$$I_{1\parallel}^{(m,2)} \propto K_{1\parallel}^{(m,2)} = (k_x^2 - 3k_y^2)(k_y^2 - 3k_x^2)k_x k_y k_z. \quad (28)$$

If, instead, the four atoms in the unit cell possess oppositely oriented local magnetic moments pointing perpendicular to the lonsdaleite main axis (see Fig. 3), the system acquires a magnetic quadrupole density that yields the orthorhombic space group $Cmc'm$ (No. 63.460), and the point-group symmetry is reduced from $D_{6h} \times C_\theta$ to $D_{2h}(C_{2v})$. The latter group possesses only one-dimensional IRs so that the two-dimensional IRs Γ_5^- and Γ_6^- of $D_{6h} \times C_\theta$ split into one-dimensional IRs of $D_{2h}(C_{2v})$. More specifically, we have

$$D_{6h} \times C_\theta \mapsto D_{2h}(C_{2v}) : \Gamma_5^- \mapsto \Gamma_1 + \Gamma_2, \quad (29)$$

which includes the identity representation Γ_1 . The lowest-order tensor operators transforming according to these IRs are listed in Table VIII. Quadrupolar magnetic order is signaled in this case by a nonzero expectation value of

$$I_{1\perp}^{(m,2)} \propto K_{1\perp}^{(m,2)} = k_x. \quad (30)$$

Table VIII also includes the compatibility relations for a magnetotoroidal dipole ($\ell = 1$) that has the same signature $--$ as the magnetic quadrupole density. For the magnetic order depicted in Fig. 2(k) when the symmetry group is $D_{6h}(D_6)$, a magnetotoroidal dipole transforms according to the IRs Γ_2 and Γ_5 of $D_{6h}(D_6)$ so that it remains forbidden. If we instead have the magnetic order depicted in Fig. 3 and the symmetry group is $D_{2h}(C_{2v})$, a magnetotoroidal dipole transforms according to the IRs Γ_1 , Γ_2 , and Γ_4 . The presence of magnetotoroidal order is thus signaled by a nonzero expectation value of the same operator (30) that also signals the presence of quadrupolar magnetic order.

TABLE VIII. Irreducible representations (IRs) and their lowest-order representative basis functions of a magnetic quadrupole and polar-toroidal vector (signatures $--$) in a hexagonal crystalline environment. The IRs are labeled according to Koster *et al.* [45]. For C_{2v} , however, the main axes x, y, z have been permuted cyclically. Basis functions shown in square brackets do not have the required transformation behavior under TIS but are included for comparison.

$R_{i \times \theta} \rightarrow R_i$	$D_2^{--} \rightarrow D_2^-$			$D_1^{--} \rightarrow D_1^-$		
$D_{6h} \times C_\theta \rightarrow D_{6h}$	Γ_1^- $(k_x^2 - 3k_y^2)(k_y^2 - 3k_x^2)k_x k_y k_z$	+	Γ_5^- k_x, k_y	+	Γ_6^- $(k_x - ik_y)^2 k_z, (k_x + ik_y)^2 k_z$	$\Gamma_2^- + \Gamma_5^-$ $k_z \quad k_x, k_y$
$D_{6h}(D_6) \rightarrow D_6$	Γ_1 $(k_x^2 - 3k_y^2)(k_y^2 - 3k_x^2)k_x k_y k_z$		Γ_5 k_x, k_y		Γ_6 $(k_x - ik_y)^2 k_z, (k_x + ik_y)^2 k_z$	$\Gamma_2 \quad \Gamma_5$ $k_z \quad k_x, k_y$
$D_{2h}(C_{2v}) \rightarrow C_{2v}$	Γ_3 $k_x k_y k_z$		$\Gamma_1 + \Gamma_2$ $k_x; [k_y^2, k_z^2] \quad k_y$		$\Gamma_3 + \Gamma_4$ $k_x k_y k_z \quad k_z$	$\Gamma_4 \quad \Gamma_1 + \Gamma_2$ $k_z \quad k_x \quad k_y$

G. Magnetization in lonsdaleite

A magnetic dipole density (magnetization) representing ferromagnetism in lonsdaleite is analyzed in Table VII. Under the point group D_{6h} of nonmagnetic lonsdaleite, the dipole density transforms according to the IRs Γ_2^+ and Γ_5^+ . Local magnetic moments on the four atoms in the unit cell pointing parallel to the main axis of lonsdaleite [Fig. 2(l)] yield the magnetic space group $P6_3/m m' c'$ (No. 194.270), and the point group becomes $D_{6h}(C_{6h}) = D_6(C_6) \times C_i$. The system is thus magnetopolar. As to be expected, the spin operator $(\hbar/2)\sigma_z$ transforms according to Γ_1^+ , and a nonzero expectation value of σ_z signals the presence of ferromagnetic order. A magnetization pointing perpendicular to the main axis of lonsdaleite can be discussed similarly.

H. Correspondence between electric and magnetic order

Figure 2 shows that, for each ℓ , the macroscopic multipole densities are realized by the same spatial pattern of electric (central row) and magnetic (bottom row) atomic multipole moments. The close connection between electric and magnetic order is also reflected by the crystallographic point groups characterizing the different structures (Table III). For odd ℓ , the point group characterizing the magnetopolar case is obtained from the group characterizing the electropolar case by replacing space inversion i by time inversion θ . On the other hand, the space group symmetries of the structures considered in Fig. 2 are quite different; all magnetic structures in the bottom row of Fig. 2 have nonsymmorphic space groups, whereas pristine lonsdaleite is the only nonsymmorphic space group in the central row.

The only exception to the correspondence between electric and magnetic order occurs for $\ell = 4$, when antimagnetopolar order with $\ell = 4$ can be realized as shown in Fig. 2(i) (all magnetic multipole densities with $\ell \leq 3$ vanish for that structure), whereas the analogous electrically ordered structure shown in Figs. 2(a)

and 2(e) (space group D_{3d}^3 , No. 164, point group $D_{3d} = D_3 \times C_i$) possesses not only an electric hexadecapolarization but also a quadrupolarization as in pristine lonsdaleite [Figs. 2(c) and 2(g)]. This is the reason why panels (a) and (e) have been separated in Fig. 2. In fact, only cubic crystal structures do not permit an electric quadrupolarization [8].

IV. DIAMOND FAMILY

The general theory developed in Sec. II is further elucidated by applying it to electric and magnetic order in the variants of diamond listed in Table III. Section IV A focuses on the electric hexadecapolarization that is compatible with the diamond structure and therefore exists in all its variations. The properties of electric octupolarization, quadrupolarization and dipolarization are discussed in Secs. IV B, IV D and IV E, respectively. As the concept of quasivectors turns out to be useful for understanding quadrupolarizations in diamond, Sec. IV C has been inserted to provide relevant details. Magnetopolarizations in diamond are considered in Secs IV G and IV I, with antimagnetopolarizations covered in Secs IV F and IV H. The multipolarization in $\text{Ga}_{1-x}\text{Mn}_x\text{As}$ and related (III,Mn)-V compounds is discussed in Sec. IV J. Connections between electric and magnetic orders are explored in the final subsection IV K.

We follow the same procedure as in Sec. III for analyzing electric order, i.e., TIS is ignored. Again, IRs of magnetic point groups are found by referring to their relevant nonmagnetic subgroup, and we continue to indicate the homomorphisms relating the magnetic groups with their nonmagnetic subgroups by ‘ \rightarrow ’. We also adhere to the same general outline of each subsection as described in the preamble of Sec. III.

A. Electric hexadecapolarization in pristine diamond

The cubic nonsymmorphic diamond structure is shown in Fig. 4(a). Ignoring TIS, the space group of diamond

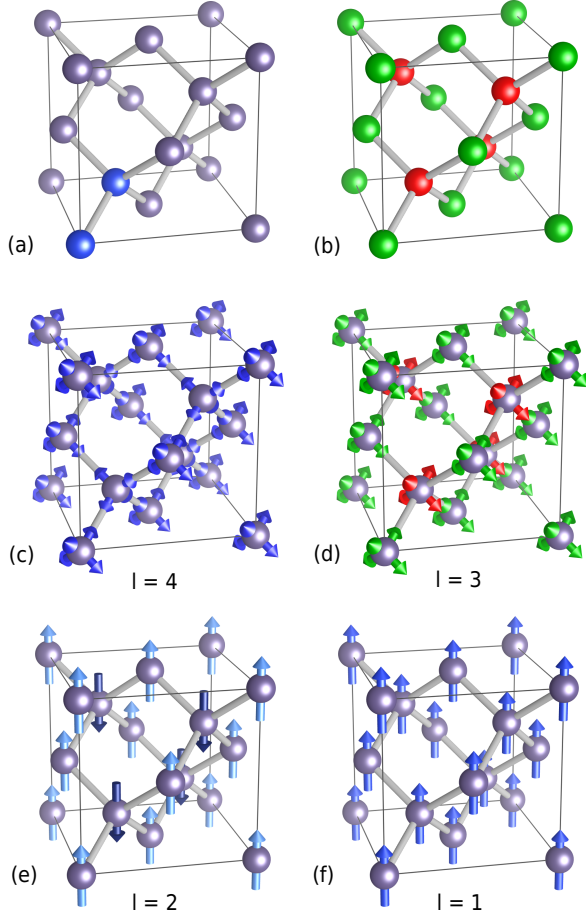


FIG. 4. Multipole densities in the diamond family. Crystal structure of (a) pristine diamond and (b) zincblende. In (a), the two atoms in a unit cell are highlighted in blue. Local octupole moments give rise to (c) a hexadecapolarization ($\ell = 4$) and (d) an octupolarization ($\ell = 3$). Local dipole moments give rise to (e) a quadrupolarization ($\ell = 2$) and (f) a dipolarization ($\ell = 1$).

is O_h^7 (No. 227, $Fd\bar{3}m$) and the crystallographic point group is $O_h = O \times C_i$, i.e., diamond is parapolar. The lowest nonvanishing electric multipole density allowed by O_h is an electric hexadecapole density ($\ell = 4$) with compatibility relation [45]

$$R_i \mapsto O_h : D_4^+ \mapsto \Gamma_1^+ + \Gamma_3^+ + \Gamma_4^+ + \Gamma_5^+. \quad (31)$$

In lowest order of the wave vector \mathbf{k} , the scalar operator associated with the hexadecapole density is the term

$$H^{(e,4)} = a^{(e,4)} \mathbf{m}^{(e,4)} (k_x^2 k_y^2 + k_y^2 k_z^2 + k_z^2 k_x^2) \quad (32)$$

that represents the warping of the energy dispersion $E_\sigma(\mathbf{k})$ of band electrons in the cubic diamond structure [92, 93].

The site symmetry of the atoms forming the diamond structure is the group T_d [37] that permits a local electric octupole moment [45]. Similar to lonsdaleite

(Sec. III A), the octupole moment is naturally realized by the sp^3 hybrid orbitals with which elements like C, Si, and Ge form the diamond structure [Fig. 4(c)]. Therefore, the invariant (32) exists already in a simple sp^3 TB model. Using the notation of Refs. [94, 95], in lowest order of the TB matrix elements V_{xy} and V_{sp} , we have $a^{(e,4)} \mathbf{m}^{(e,4)} \propto V_{xy}^2 V_{sp}^2$.

The lowest electrotoroidal moment permitted in diamond has $\ell = 9$.

B. Electric octupolarization in diamond – zincblende

The unit cell of pristine diamond contains two identical atoms [Fig. 4(a)]. If these two atoms are distinct, we obtain the zincblende structure [Fig. 4(b)] that is realized by several III-V semiconductors including GaAs and InSb. The space group of zincblende is T_d^2 (No. 216, $F\bar{4}3m$), and the crystallographic point group is T_d . Unlike $O_h = T_d \times C_i$, the group T_d breaks SIS so that zincblende is electropolar. More specifically, the compatibility relation [45]

$$R_i \mapsto T_d : D_3^- \mapsto \Gamma_1 + \Gamma_5 + \Gamma_4 \quad (33)$$

indicates that zincblende naturally permits an electric octupole density ($\ell = 3$). The corresponding invariant in the Hamiltonian (to lowest order in \mathbf{k}) is

$$H^{(e,3)} = a^{(e,3)} \mathbf{m}^{(e,3)} [\sigma_x k_x (k_y^2 - k_z^2) + \text{cp}] , \quad (34)$$

where “cp” denotes cyclic permutation of the preceding term. The invariant $H^{(e,3)}$ represents a spin-orbit coupling commonly known as Dresselhaus term [33].

A more complete analysis of the electric octupole density in zincblende is given in Table IX. Ignoring TIS, the octupole density transforms according to D_3^- of R_i . A cubic environment (point group O_h) yields the compatibility relation [45]

$$R_i \mapsto O_h : D_3^- \mapsto \Gamma_2^- + \Gamma_4^- + \Gamma_5^-, \quad (35)$$

so that, as to be expected, an octupole density is forbidden in diamond. The lowest-order tensor operator with signature $-+$ and transforming like Γ_2^- is

$$K_{2-}^{(e,3)} = \sigma_x k_x (k_y^2 - k_z^2) + \text{cp}. \quad (36)$$

Examples of tensor operators transforming like Γ_4^- and Γ_5^- are listed in Table IX. The expectation value of these operators must thus vanish in diamond. When the symmetry is further reduced to T_d (zincblende), we get the compatibility relation [45]

$$O_h \mapsto T_d : \Gamma_2^- \mapsto \Gamma_1, \quad \Gamma_4^- \mapsto \Gamma_5, \quad \Gamma_5^- \mapsto \Gamma_4, \quad (37)$$

so that the tensor operator (36) becomes allowed and yields the Dresselhaus term (34).

TABLE IX. Irreducible representations (IRs) and their lowest-order representative basis functions of an electric (signature $-+$) and a magnetic (signature $+ -$) octupole in a cubic crystalline environment. The IRs are labeled according to Koster *et al.* [45]. Basis functions listed for the IRs of O_h are also basis functions for the respective IRs of T_d . “cp” denotes the cyclic permutation of the preceding term.

$R_{i \times \theta} \rightarrow R_i$	$D_3^{-+} \rightarrow D_3^-$		
$O_h \times C_\theta \rightarrow O_h$	Γ_2^- $\sigma_x k_x (k_y^2 - k_z^2) + \text{cp}$	+	Γ_4^- $\sigma_y k_z - \sigma_z k_y, \sigma_z k_x - \sigma_x k_z, \sigma_x k_y - \sigma_y k_x$
$T_d \times C_\theta \rightarrow T_d$	Γ_1		Γ_5^- $\sigma_y k_z + \sigma_z k_y, \sigma_z k_x + \sigma_x k_z, \sigma_x k_y + \sigma_y k_x$
$R_{i \times \theta} \rightarrow R_i$	$D_3^{+-} \rightarrow D_3^+$		
$O_h \times C_\theta \rightarrow O_h$	Γ_2^+ $\sigma_x k_y k_z + \text{cp}$	+	Γ_4^+ $\sigma_x, \sigma_y, \sigma_z$
$O_h(T_h) \rightarrow T_h$	Γ_1^+		Γ_5^+ $\sigma_x (k_y^2 - k_z^2), \sigma_y (k_z^2 - k_x^2), \sigma_z (k_x^2 - k_y^2);$

The site symmetry of the atoms is, once again, T_d [37]. However, similar to wurtzite, the two distinct atoms in Fig. 4(b) have different Wyckoff positions, and they may carry different electric octupole moments. Again, we decompose these moments $\mathcal{M} \equiv \mathcal{M}_0 + \Delta\mathcal{M}$ into one part \mathcal{M}_0 that is equal by symmetry for all atoms as in diamond. These moments thus have the same observable effect as the local moments in pristine diamond [Fig. 4(c)], i.e., they give rise to the invariant (32). It is the remaining part $\Delta\mathcal{M}$ oriented oppositely that is shown in Fig. 4(d) and that gives rise to the Dresselhaus term (34).

The lowest electrotoroidal moment permitted in zincblende has $\ell = 6$.

The standard sp^3 TB model for zincblende [94, 95] provides an explicit model for Dresselhaus spin-orbit coupling (34) and its relation to the octupolarization in zincblende. The TB model accounts for the different atomic species constituting zincblende structures with different on-site energies for anions and cations; we denote their difference with ΔE_j^{ac} , $j = s, p$. Also, we get different overlap matrix elements $V_{sp\sigma}$ between, on the one hand, the anion s and cation p orbitals and, on the other hand, the cation s and anion p orbitals. We denote the difference between these overlap matrix elements by $\Delta V_{sp\sigma}^{\text{ac}}$. This quantity represents the scalar component (IR Γ_1) of an octupolar charge transfer between anions and cations in zincblende. (Larger TB models may include multiple overlap matrix elements that permit such an interpretation.) In a perturbative expansion of the sp^3 TB model about $k = 0$, Dresselhaus spin splitting is linearly proportional to $\Delta V_{sp\sigma}^{\text{ac}}$, whereas it is only quadratically proportional to ΔE_i^{ac} . This is consistent with the $\mathbf{k} \cdot \mathbf{p}$ theory for Dresselhaus spin-orbit coupling, where it is well-known that a minimal model for Dresselhaus spin-orbit coupling in the lowest conduction band (which has s -like symmetry) must include the top-most valence band (consisting of p -bonding states in TB language) as well as the lowest excited conduction band (consisting of p -antibonding states) [93, 96].

The Dresselhaus term (34) couples the orbital motion of the Bloch electrons to the spin degree of freedom, con-

sistent with the analysis in Table IV that applies to spinful models. In spinless models of common zincblende semiconductors, the topmost valence band originating from p -bonding atomic orbitals is threefold degenerate at $k = 0$. Here, the electric octupolarization in zincblende breaking SIS manifests itself via terms in the perturbative expansion of the band structure that include odd powers of the wave vector \mathbf{k} [31].

C. Quasivectors under point group O_h

Before discussing electric quadrupole densities in diamond, we introduce the concept of *quasivectors* in systems with point group O_h . The point group O_h has four three-dimensional IRs denoted Γ_4^\pm and Γ_5^\pm in Koster’s notation [45]. Function triples like the components k_x, k_y, k_z of the wave vector \mathbf{k} that behave like a polar vector under all symmetry elements of O_h are ascribed the IR Γ_4^- of O_h . On the other hand, function triples such as $k_x(k_y^2 - k_z^2), k_y(k_z^2 - k_x^2), k_z(k_x^2 - k_y^2)$ transform according to the IR Γ_5^- of O_h . The latter functions behave like polar vectors under half of the symmetry elements of O_h . However, they change sign under proper $\pm\pi/2$ rotations about axes $\langle 100 \rangle$ and proper π rotations about axes $\langle 110 \rangle$, while they behave like axial vectors (not changing sign) under improper $\pm\pi/2$ rotations about axes $\langle 100 \rangle$ and improper π rotations about axes $\langle 110 \rangle$. We call sets of functions transforming according to Γ_5^- of O_h *polar quasivectors*.

Similarly, function triples like $k_y k_z (k_y^2 - k_z^2), k_z k_x (k_z^2 - k_x^2), k_x k_y (k_x^2 - k_y^2)$ behaving like axial vectors under all symmetry elements of O_h are ascribed the IR Γ_4^+ of O_h . On the other hand, function triples such as $k_y k_z, k_z k_x, k_x k_y$ transforming according to the IR Γ_5^+ of O_h behave like axial vectors under half of the symmetry elements of O_h . However, they change sign under proper $\pm\pi/2$ rotations about axes $\langle 100 \rangle$ and proper π rotations about axes $\langle 110 \rangle$, while they behave like polar vectors (changing sign) under improper $\pm\pi/2$ rotations about axes $\langle 100 \rangle$ and improper π rotations about axes

TABLE X. IRs of vectors and quasivectors under the group O_h [45]. We list the lowest-degree polynomials in wave vector \mathbf{k} and spin $\boldsymbol{\sigma}$ that are even and odd under TIS and that transform irreducibly according to these IRs.

axial vectors	Γ_4^+	$\sigma_x, \sigma_y, \sigma_z; k_y k_z (k_y^2 - k_z^2), k_z k_x (k_z^2 - k_x^2), k_x k_y (k_x^2 - k_y^2)$
axial quasivectors	Γ_5^+	$k_y k_z, k_z k_x, k_x k_y; \sigma_x (k_y^2 - k_z^2), \sigma_y (k_z^2 - k_x^2), \sigma_z (k_x^2 - k_y^2);$ $k_x (\sigma_y k_y - \sigma_z k_z), k_y (\sigma_z k_z - \sigma_x k_x), k_z (\sigma_x k_x - \sigma_y k_y)$
polar vectors	Γ_4^-	$k_x, k_y, k_z; \sigma_y k_z - \sigma_z k_y, \sigma_z k_x - \sigma_x k_z, \sigma_x k_y - \sigma_y k_x$
polar quasivectors	Γ_5^-	$\sigma_y k_z + \sigma_z k_y, \sigma_z k_x + \sigma_x k_z, \sigma_x k_y + \sigma_y k_x; k_x (k_y^2 - k_z^2), k_y (k_z^2 - k_x^2), k_z (k_x^2 - k_y^2)$

(110). We call sets of functions transforming according to Γ_5^+ of O_h *axial quasivectors*.

The IRs for vectors and quasivectors under the point group O_h are summarized in Table X. We illustrate these IRs with representative basis functions transforming according to these IRs. The table gives the lowest-degree polynomials in wave vector \mathbf{k} and spin $\boldsymbol{\sigma}$ that are even and odd under TIS. By definition, in a cubic environment (point group O_h) none of these vectors are observable. They become observable when the crystal symmetry is reduced.

D. Electric quadrupolarization in diamond

Next we discuss an electric quadrupole density in diamond. The analysis is summarized in Table XI. The cubic group O_h yields the compatibility relation [45]

$$R_i \mapsto O_h : D_2^+ \mapsto \Gamma_3^+ + \Gamma_5^+, \quad (38)$$

i.e., the five components of the quadrupole decompose into an axial quasivector (Γ_5^+) and two components transforming according to Γ_3^+ . As to be expected, an electric quadrupole is forbidden for O_h .

As in pristine lonsdaleite (Sec. III A), we consider the case that the nonzero component of the quadrupole density is $m = 0$. If the main axis of the quadrupole is parallel to the crystallographic [001] axis, the point group becomes D_{4h} and we get the compatibility relations

$$O_h \mapsto D_{4h} : \begin{cases} \Gamma_3^+ \mapsto \Gamma_1^+ + \Gamma_3^+ \\ \Gamma_5^+ \mapsto \Gamma_4^+ + \Gamma_5^+ \end{cases} \quad (39)$$

In this case we obtain the same invariant as in lonsdaleite,

$$H^{(e,2)} = a^{(e,2)} m_z^{(e,2)} K_1^{(e,2)} \quad (40a)$$

$$= a^{(e,2)} m_z^{(e,2)} (k_x^2 + k_y^2 - 2k_z^2), \quad (40b)$$

that represents an effective-mass anisotropy in the energy dispersion $E_\sigma(\mathbf{k})$ of band electrons in diamond. The axial quasivector transforming according to Γ_5^+ of O_h remains forbidden.

We compare with the case that the main axis of the quadrupole is parallel to the crystallographic [111] axis, when the point group symmetry becomes C_{2h} and we get

the compatibility relations

$$O_h \mapsto C_{2h} : \begin{cases} \Gamma_3^+ \mapsto \Gamma_1^+ + \Gamma_2^+ \\ \Gamma_5^+ \mapsto 2\Gamma_1^+ + \Gamma_2^+ \end{cases} \quad (41)$$

Here the IR Γ_1 appears three times so that the quadrupole density has three independent components, two of which represent the axial quasivector (Γ_5^+) in the decomposition (38) of the quadrupole density.

Table XI also includes the compatibility relations for an electrotoroidal dipole ($\ell = 1$) that has the same signature $++$ as the electric quadrupole density. In the language of Sec. IV C, the electrotoroidal dipole is an axial vector, whereas the electric quadrupole density includes a part transforming like an axial quasivector [Eq. (38)]. When the symmetry is reduced from O_h to D_{4h} , the electrotoroidal dipole remains forbidden. On the other hand, the reduced symmetry C_{2h} implies that not only the axial quasivector (Γ_5^+ of O_h) becomes allowed for C_{2h} [Eq. (41)], but also an axial vector (Γ_4^+ of O_h) becomes observable

$$O_h \mapsto C_{2h} : \Gamma_4^+ \mapsto \Gamma_1^+ + 2\Gamma_2^+. \quad (42)$$

It becomes clear from Table XI that the reason for the observability of both quantities under C_{2h} lies in the fact that axial vectors and axial quasivectors are only distinct quantities under the high symmetry of the point group O_h . But they represent the same observable physics when the symmetry is reduced to a group like C_{2h} that makes both of these quantities measurable. Both quantities manifest themselves via terms in the energy dispersion of band electrons proportional to the invariants $k_z k_x$ and $k_z k_x (k_z^2 - k_x^2)$.

1. Strain

An electric quadrupole density becomes allowed in diamond when the symmetry is reduced by means of strain [76] or quantum confinement [31]. Similar to an electric quadrupole density, in cartesian coordinates strain is characterized via a symmetric rank-2 tensor ϵ [97]. The trace of ϵ represents the effect of hydrostatic pressure. Ignoring hydrostatic pressure, the tensor ϵ is traceless. The effect of strain [52] is then equivalent to inducing an electric quadrupole density. A nonzero component ϵ_{ij} implies that the respective component of the electric quadrupole density becomes observable, too.

TABLE XI. Irreducible representations (IRs) and their lowest-order representative basis functions of an electric quadrupole and axial-toroidal vector (signatures ++) in a cubic crystalline environment. The IRs are labeled according to Koster *et al.* [45].

$R_{i \times \theta} \rightarrow R_i$	$D_2^{++} \rightarrow D_2^+$		$D_1^{++} \rightarrow D_1^+$		
$O_h \times C_\theta \rightarrow O_h$	Γ_3^+	+	Γ_5^+	Γ_4^+	
	$(2k_z^2 - k_x^2 - k_y^2), \sqrt{3}(k_x^2 - k_y^2)$		$k_y k_z, k_z k_x, k_x k_y$	$k_y k_z (k_y^2 - k_z^2), k_z k_x (k_z^2 - k_x^2), k_x k_y (k_x^2 - k_y^2)$	
[001] : D_{4h}	Γ_1^+	+	Γ_4^+	+	Γ_5^+
	$k_x^2 + k_y^2; k_z^2$	$k_x^2 - k_y^2$	$k_x k_y$	$k_y k_z, k_z k_x$	$k_x k_y (k_x^2 - k_y^2), k_y k_z (k_y^2 - k_z^2), k_z k_x (k_z^2 - k_x^2)$
[mmn] : C_{2h}	Γ_1^+	+	$2\Gamma_1^+$	+	$2\Gamma_2^+$
	$k_x^2; k_y^2; k_z^2; k_z k_x$	$k_x k_y; k_y k_z$	$k_x^2; k_y^2; k_z^2; k_z k_x$	$k_x k_y; k_y k_z$	$k_x^2; k_y^2; k_z^2; k_z k_x$

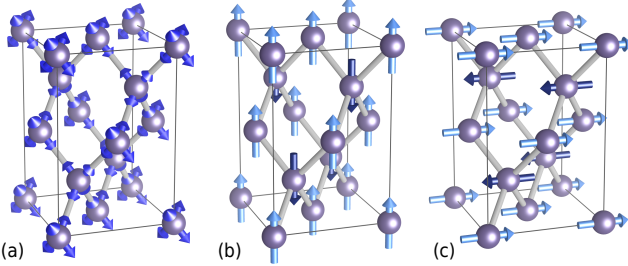


FIG. 5. Quadrupole densities in tetragonally distorted diamond. (a) The distorted electric octupole moments due to the sp^3 hybrid orbitals give rise to local electric quadrupole moments which, in turn, give rise to an electric quadrupole density. Alternating patterns of magnetic dipole moments oriented (b) parallel and (c) perpendicular to the tetragonal axis give rise to magnetic quadrupole densities.

The strain due to uniaxial stress applied in [001] direction reduces the space group of diamond to the tetragonal group D_{4h}^{19} (No. 141, $I4_1/amd$) with point group D_{4h} . The site symmetry of the atoms becomes D_{2d} that supports an electric quadrupole moment [Fig. 5(a)].

E. Electric dipolarization in zincblende

Similar to wurtzite, an electric dipole density becomes allowed if the symmetry of diamond is reduced from O_h to one of the polar subgroups of O_h including C_{4v} , C_{3v} , and C_{2v} . This is summarized in Table XII. In these cases, the dipole density manifests itself via the same Rashba term (17) as in wurtzite. Starting from a bulk zincblende structure, the polar point groups C_{3v} and C_{2v} can be obtained experimentally by applying uniaxial strain in the crystallographic direction [111] (C_{3v}) or [110] (C_{2v}), which is the familiar piezoelectric effect [8] that exists for zincblende structures (but not for diamond). It has been noted previously [98, 99] that for systems with point groups C_{3v} and C_{2v} , the Dresselhaus term takes the form of a Rashba term linear in the wave vector \mathbf{k} . Indeed, this is due to the fact that the system becomes polar and possesses an electric dipole density.

TABLE XII. Irreducible representations (IRs) and their lowest-order representative basis functions of an electric dipole (signature -+) and magnetic dipole (signature +-) in a cubic crystalline environment. The IRs are labeled according to Koster *et al.* [45].

$R_{i \times \theta} \rightarrow R_i$	$D_1^{-+} \rightarrow D_1^-$		
$O_h \times C_\theta \rightarrow O_h$	Γ_4^-		
	$\sigma_y k_z - \sigma_z k_y, \sigma_z k_x - \sigma_x k_z, \sigma_x k_y - \sigma_y k_x$		
$T_d \times C_\theta \rightarrow T_d$	Γ_5		
	$\sigma_y k_z - \sigma_z k_y, \sigma_z k_x - \sigma_x k_z, \sigma_x k_y - \sigma_y k_x$		
[001] : C_{4v}	Γ_1	+	Γ_5
	$\sigma_x k_y - \sigma_y k_x$	$\sigma_y k_z - \sigma_z k_y, \sigma_z k_x - \sigma_x k_z$	
[111] : C_{3v}	Γ_1	+	Γ_3
	$\sigma_x k_y - \sigma_y k_x$	$\sigma_y k_z - \sigma_z k_y, \sigma_z k_x - \sigma_x k_z$	
[110] : C_{2v}	Γ_1	+	Γ_2 + Γ_4
	$\sigma_x k_y; \sigma_y k_x$	$\sigma_y k_z; \sigma_z k_y$	$\sigma_x k_z; \sigma_z k_x$

$R_{i \times \theta} \rightarrow R_i$	$D_1^{+-} \rightarrow D_1^+$		
$O_h \times C_\theta \rightarrow O_h$	Γ_4^+		
	$\sigma_x, \sigma_y, \sigma_z$		
[001] : $D_{4h}(C_{4h}) \rightarrow C_{4h}$	Γ_1^+	+	$\Gamma_3^+ + \Gamma_4^+$
	σ_z	σ_x, σ_y	

F. Magnetic hexadecapolarization in diamond

In analogy with the electric hexadecapole density characterizing pristine diamond (Sec. IV A) and the octupole density characterizing the zincblende structure (Sec. IV B), we can also discuss magnetic multipole densities that can be modeled using atomic octupoles on the two sublattices of diamond as the elementary building blocks for the multipolar order [36]. When going from the rotation group $R_{i \times \theta} \rightarrow R_i$ to $O_h \times C_\theta \rightarrow O_h$, the compatibility relation for a magnetic hexadecapole $D_4^{--} \rightarrow D_4^-$ reads

$$R_i \mapsto O_h : D_4^- \mapsto \Gamma_1^- + \Gamma_3^- + \Gamma_4^- + \Gamma_5^-, \quad (43)$$

hence the hexadecapole remains forbidden. If local magnetic octupoles on the two sublattices of diamond are

oriented as in Fig. 4(c), they reduce the symmetry of diamond to the space group $Fd\bar{3}m'$ (No. 227.132), and the point group becomes

$$O_h(O) = O \times C_{i\theta} \rightarrow O, \quad (44)$$

i.e., the system becomes antimagnetopolar. More specifically, we get the compatibility relations

$$O_h \mapsto O: \quad \Gamma_1^- \mapsto \Gamma_1, \Gamma_3^- \mapsto \Gamma_3, \Gamma_4^- \mapsto \Gamma_4, \Gamma_5^- \mapsto \Gamma_5. \quad (45)$$

Under $O_h(O)$, hexadecapolar magnetic order is signaled by a nonzero expectation value of the indicator

$$I_1^{(m,4)} \propto K_1^{(m,4)} = k_x k_y k_z (k_y^2 - k_z^2)(k_z^2 - k_x^2)(k_x^2 - k_y^2). \quad (46)$$

Like the Dresselhaus term (34), $I_1^{(m,4)}$ exhibits cubic symmetry.

Incidentally, the group $O_h(O)$ also permits a magnetic monopole density ($\ell = 0$)

$$R_i \mapsto O_h \mapsto O: \quad D_0^- \mapsto \Gamma_1^- \mapsto \Gamma_1 \quad (47)$$

that gives rise to the same observable physics as the hexadecapole density. In Ref. [14], the indicator (46) was associated with a magnetic monopolarization.

The site symmetry of the magnetic sites in Fig. 4(c) is $T_d(T)$ that supports a magnetic octupole moment. Similar to the invariant (13) in lonsdaleite, Eq. (46) can already be evaluated in a simple sp^3 TB model for diamond [94, 95]. Local magnetic octupole moments can be implemented as a spin Zeeman term for the four sp^3 orbitals on each site, assuming that the exchange field complementing each sp^3 orbital is oriented along the respective orbital. A perturbative expansion of the resulting TB model includes a term $\propto K_1^{(m,4)}$ from Eq. (46).

A magnetic hexadecapolarization has previously been discussed for a particular materials system [100].

G. Magnetic octupolarization in diamond

If the orientation of the atomic magnetic octupoles on one of the diamond sublattices is reversed as in Fig. 4(d), these octupoles give rise to a macroscopic magnetic octupole density whose symmetry properties are summarized in Table IX. When going from the rotation group $R_{i \times \theta} \rightarrow R_i$ to $O_h \times C_\theta \rightarrow O_h$, the compatibility relation for a magnetic octupole $D_3^{+} \rightarrow D_3^{+}$ reads

$$R_i \mapsto O_h: \quad D_3^{+} \mapsto \Gamma_2^{+} + \Gamma_4^{+} + \Gamma_5^{+}, \quad (48)$$

hence the octupole remains forbidden. The lowest-order tensor operators transforming according to the IRs Γ_2^{+} , Γ_4^{+} , and Γ_5^{+} of O_h and consistent with the signature $+-$ of a magnetic octupole density are listed in Table IX.

The magnetic octupole density illustrated in Fig. 4(d) reduces the symmetry of diamond to the space group $Fd\bar{3}m'$ (No. 227.131), and the point group becomes

$$O_h(T_h) = O(T) \times C_i \rightarrow T_h = T \times C_i, \quad (49)$$

i.e., the system becomes magnetopolar. More specifically, we get the compatibility relations

$$O_h \mapsto T_h: \quad \Gamma_2^{+} \mapsto \Gamma_1^{+}, \Gamma_4^{+} \mapsto \Gamma_4^{+}, \Gamma_5^{+} \mapsto \Gamma_5^{+}. \quad (50)$$

Therefore, under $O_h(T_h)$ octupolar magnetic order is signaled by a nonzero expectation value of

$$I_1^{(m,3)} \propto K_1^{(m,3)} = \sigma_x k_y k_z + \sigma_y k_z k_x + \sigma_z k_x k_y. \quad (51)$$

Unlike Eq. (25) in lonsdaleite, but similar to the Dresselhaus term (34), this term preserves the cubic symmetry and can thus be viewed as a generalized form of altermagnetism [79] without a global spin-quantization axis.

The site symmetry of the local magnetic moments in Fig. 4(d) is again $T_d(T)$. The magnetic octupolarization can be implemented in an sp^3 TB model as described in Sec. IV F for the magnetic hexadecapolarization, but by giving opposite signs to the local octupole moments on the two sublattices.

H. Magnetic quadrupolarization in diamond

A magnetic quadrupole density is illustrated in Fig. 4(e) [101]. Recently, such a quadrupole density has been analyzed in Ref. [66]. Here we present a more detailed discussion that is summarized in Table XIII. When going from the rotation group $R_{i \times \theta} \rightarrow R_i$ to $O_h \times C_\theta \rightarrow O_h$, the compatibility relation for a magnetic quadrupole $D_2^{-} \rightarrow D_2^{-}$ reads

$$R_i \mapsto O_h: \quad D_2^{-} \mapsto \Gamma_3^{-} + \Gamma_5^{-}, \quad (52)$$

i.e., the quadrupole remains forbidden. The lowest-order tensor operators transforming according to the IRs Γ_3^{-} and Γ_5^{-} and consistent with the signature $--$ of a magnetic quadrupole density are listed in Table XIII. In Ref. [66], the indicator associated with Γ_5^{-}

$$I_{5-}^{(m,2)} \propto K_{5-}^{(m,2)} = \begin{pmatrix} k_x(k_y^2 - k_z^2) \\ k_y(k_z^2 - k_x^2) \\ k_z(k_x^2 - k_y^2) \end{pmatrix} \quad (53)$$

was called Néel operator, and it was argued that a nonzero expectation value of this quantity signals the presence of AFM order in the magnetic diamond structure shown in Fig. 4(e). The concept of indicators introduced in Eq. (7) extends this idea to different types of electric and magnetic multipolar order in crystal structures.

The diamond structure with locally alternating magnetic dipoles [Fig. 4(e)] reduces the space group symmetry to $I4_1'/a'm'd$ (No. 141.566), and the magnetic point group becomes $D_{4h}(D_{2d}) = D_4(D_2) \times C_{i\theta} \rightarrow D_{2d}$ so that the system is antimagnetopolar. More specifically, we get the compatibility relations

$$O_h \mapsto D_{2d}: \quad \begin{cases} \Gamma_3^{-} \mapsto \Gamma_3 + \Gamma_3 \\ \Gamma_5^{-} \mapsto \Gamma_1 + \Gamma_5. \end{cases} \quad (54)$$

TABLE XIII. Irreducible representations (IRs) and their lowest-order representative basis functions of a magnetic quadrupole and polar-toroidal vector (signatures $--$) in a cubic crystalline environment. The IRs are labeled according to Koster *et al.* [45]. For D_{2d} , however, Koster's coordinate system has been rotated by $\pi/4$ about the main axis of D_{2d} , which changes the representative basis functions for the IRs Γ_2 , Γ_3 , and Γ_4 of D_{2d} . For C_{2v} , the main axes x, y, z have been permuted cyclically. Basis functions shown in square brackets do not have the required transformation behavior under TIS, but are included for comparison.

$R_{i \times \theta} \rightarrow R_i$	$D_2^- \rightarrow D_2^-$		$D_1^- \rightarrow D_1^-$		
$O_h \times C_\theta \rightarrow O_h$	Γ_3^- $(2k_x^2 - k_x^2 - k_y^2)k_x k_y k_z,$ $\sqrt{3}(k_x^2 - k_y^2)k_x k_y k_z$	+	Γ_5^- $k_x(k_y^2 - k_z^2), k_y(k_z^2 - k_x^2), k_z(k_x^2 - k_y^2)$	Γ_4^- k_x, k_y, k_z	
$D_{4h}(D_{2d}) \rightarrow D_{2d}$	Γ_2 $k_x k_y k_z$	+	Γ_3 $(k_x^2 - k_y^2)k_x k_y k_z$	Γ_1 + Γ_5 $k_z(k_x^2 - k_y^2);$ $[k_z^2; k_x^2 + k_y^2]$ $k_x(k_y^2 - k_z^2), k_y(k_z^2 - k_x^2);$ k_x, k_y	Γ_4 + Γ_5 $k_z;$ $[k_x^2 - k_y^2]$ k_x, k_y
$D_{4h} \times C_\theta \rightarrow D_{4h}$	Γ_1^- $(k_x^2 - k_y^2)k_x k_y k_z$	+	Γ_3^- $k_x k_y k_z$	Γ_4^- + Γ_5^- $k_z(k_x^2 - k_y^2)$ $k_x(k_y^2 - k_z^2), k_y(k_z^2 - k_x^2);$ k_x, k_y	Γ_2^- + Γ_5^- k_z k_x, k_y
$D_{2h}(C_{2v}) \rightarrow C_{2v}$	Γ_3 $k_x k_y k_z$	Γ_3 $k_x k_y k_z$	Γ_4 k_z	Γ_1 + Γ_2 $k_x; [k_y^2; k_z^2]$ k_y	Γ_4 k_z $\Gamma_1 + \Gamma_2$ $k_x \quad k_y$

Therefore, under $D_{4h}(D_{2d})$, quadrupolar magnetic order is signaled by a nonzero expectation value of

$$D_{4h}(D_{2d}) : I_1^{(m,2)} \propto K_1^{(m,2)} = k_z(k_x^2 - k_y^2). \quad (55)$$

As discussed in Ref. [66], the locally alternating magnetic dipoles [Fig. 4(e)] can be implemented in an sp^3 TB model [94, 95] as a local exchange field that is oriented oppositely on the two sublattices of diamond. A perturbative expansion of the TB model to lowest order in \mathbf{k} then yields a term proportional to the right-hand-side of Eq. (55).

1. Magnetic quadrupolarization in quantum-confined diamond

As discussed in Sec. IV D, an electric quadrupole density that may be realized via uniaxial strain or quantum confinement can reduce the symmetry of diamond from O_h to D_{4h} . Reference [66] studied a magnetic quadrupole density for this scenario, and we want to review the case using the language developed in the present work. We assume that the uniaxial strain is oriented in the crystallographic [001] direction, which is symmetry-wise equivalent to a quantum well grown on a (001) surface. When going from the rotation group $R_{i \times \theta} \rightarrow R_i$ to $D_{4h} \times C_\theta \rightarrow D_{4h}$, the compatibility relation for a magnetic quadrupole $D_2^- \rightarrow D_2^-$ reads

$$R_i \mapsto D_{4h} : D_2^- \mapsto \Gamma_1^- + \Gamma_3^- + \Gamma_4^- + \Gamma_5^-. \quad (56)$$

If the alternating magnetic moments on the two diamond sublattices point parallel to the [001] direction [Fig. 5(b)], the magnetic point group is reduced from $D_{4h} \times C_\theta$ to once again $D_{4h}(D_{2d})$ that was already

discussed above. If the moments point parallel to the [100] direction [Fig. 5(c)], the symmetry group becomes $D_{2h}(C_{2v}) \rightarrow C_{2v}$. The compatibility relations are

$$D_{4h} \mapsto C_{2v} : \begin{cases} \Gamma_1^- \mapsto \Gamma_3 \\ \Gamma_3^- \mapsto \Gamma_3 \\ \Gamma_4^- \mapsto \Gamma_4 \\ \Gamma_5^- \mapsto \Gamma_1 + \Gamma_2, \end{cases} \quad (57)$$

with representative basis functions listed in Table XIII. Thus under $D_{2h}(C_{2v})$, quadrupolar magnetic order becomes once again allowed, and its presence is signaled by a nonzero expectation value of [66]

$$D_{2h}(C_{2v}) : I_1^{(m,2)} \propto K_1^{(m,2)} = k_x. \quad (58)$$

Table XIII also includes the compatibility relations for a magnetotoroidal dipole ($\ell = 1$) that has the same signature $--$ as the magnetic quadrupole density. In the language of Sec. IV C, under $O_h \times C_\theta \rightarrow O_h$ the magnetotoroidal dipole is a polar vector (IR Γ_4^-), whereas the magnetic quadrupole density includes a part transforming like a polar quasivector [IR Γ_5^- , Eq. (52)]. When the symmetry is reduced from $O_h \times C_\theta$ to $D_{4h}(D_{2d})$, the polar quasivector becomes allowed, but the polar vector remains forbidden. On the other hand, the reduced symmetry $D_{2h}(C_{2v})$ implies that not only a polar quasivector (Γ_5^- of O_h) becomes allowed [Eq. (57)], but also a polar vector (Γ_4^- of O_h) becomes observable

$$O_h \mapsto C_{2v} : \Gamma_4^- \mapsto \Gamma_4 + \Gamma_1 + \Gamma_2. \quad (59)$$

It becomes clear from Table XIII that the reason for the observability of both vectors under $D_{2h}(C_{2v})$ lies in the fact that polar vectors and polar quasivectors are only distinct quantities under high-symmetry point groups

like $O_h \times C_\theta$ and $D_{4h}(D_{2d})$. But they represent the same observable physics when the symmetry is reduced to a group like $D_{2h}(C_{2v})$ that makes both of these quantities measurable. Under $D_{2h}(C_{2v})$, both quantities manifest themselves via terms in the energy dispersion of band electrons proportional to the invariant k_x [Eq. (58)].

I. Magnetization in diamond

A magnetic dipole density representing ferromagnetic order in diamond is analyzed in Table XII. Under the point group O_h of nonmagnetic diamond, the dipole density transforms according to the IR Γ_4^+ . A magnetization pointing parallel to the crystallographic direction [001] [Fig. 4(f)] reduces the symmetry to $D_{4h}(C_{4h}) \rightarrow C_{4h}$. As to be expected, the spin operator σ_z transforms according to Γ_1^+ of C_{4h} and a nonzero expectation value of σ_z signals the presence of ferromagnetic order.

J. Multipolarization in $\text{Ga}_{1-x}\text{Mn}_x\text{As}$

Ferromagnetic $\text{Ga}_{1-x}\text{Mn}_x\text{As}$ and related (III,Mn)-V compounds [102] are examples for multipolar materials. Above the Curie temperature, $\text{Ga}_{1-x}\text{Mn}_x\text{As}$ has a zincblende structure (Sec. IV B). Below the critical temperature, it has the magnetic space group $I\bar{4}m'2'$ (No. 119.319) and point group $D_{2d}(S_4)$. It inherits the electric octupolarization ($\ell = 3$) of the parent zincblende structure that manifests itself via the Dresselhaus term (34), i.e., this material is electropolar. Mn gives rise to a magnetopolarization parameterized by a Zeeman-like exchange term (Table XII). But $\text{Ga}_{1-x}\text{Mn}_x\text{As}$ also supports an antimagnetopolarization ($\ell = 2$) parameterized by a term as in Eq. (55) [66]. In a TB model [94, 95], this term can be traced back to the fact that, unlike the ferromagnetic structure in Fig. 4(f), the two sublattices of the diamond structure are distinct in $\text{Ga}_{1-x}\text{Mn}_x\text{As}$. Similarly, ferrimagnets are often multipolar.

K. Correspondence between electric and magnetic order

Similar to lonsdaleite, electric and magnetic order in variants of diamond follows a close correspondence. Figures 4(c) and 4(d) represent hexadecapolar and octupolar order due to local octupole moments for both the electric and the magnetic case. As summarized in Table III, for odd ℓ , the point group characterizing the magnetopolar case is obtained from the group characterizing the electropolar case by replacing space inversion i by time inversion θ .

V. CONCLUSIONS AND OUTLOOK

Using symmetry, we have developed a general theory of electric, magnetic, and toroidal polarizations in crystalline solids. We have identified four families of multipole densities representing even- ℓ and odd- ℓ electric and magnetic multipoles (Table II). Beyond the standard distinction between electric and magnetic multipoles, each of these four families bring about qualitatively different physics as they behave differently under space inversion i and time inversion θ . The four families of multipole densities give rise to five qualitatively distinct categories of polarized matter (Table II). Even- ℓ electric multipole densities may exist in all categories of polarized matter; they are the only family of multipole densities permitted in parapolar media. Electropolar, magnetopolar, and antimagnetopolar media permit each exactly one other family of multipole densities, while multipolar media permit all four families of multipole densities. Each category is characterized by distinct features in the band structure of Bloch electrons (Fig. 1).

Our group-theoretical analysis does not reference electromagnetism to define multipolar order. In this way, it avoids the difficulties underlying an electromagnetic definition of multipole densities as the multipole moment of an arbitrarily chosen unit cell. Group theory is used, in particular, to derive the invariants (6) that incorporate the effect of electric and magnetic multipolar order into the Hamiltonian for the dynamics of Bloch electrons. Nonetheless, in quantum-confined geometries, the invariants (6) reproduce the electromagnetic hallmarks of electric and magnetic multipole densities including, e.g., equilibrium currents representing a magnetization ($\ell = 1$) or magnetic quadrupolarization ($\ell = 2$), as demonstrated in a recent study of the magnetoelectric effect in quasi-2D systems [66].

Our analysis reveals that the familiar Rashba SO coupling (17) represents the electric dipolarization in electropolar materials such as wurtzite. Rashba SO coupling has been the starting point for countless fundamental studies and applications that have greatly stimulated the field of spintronics [103, 104]. Beyond that, our work establishes a systematic correspondence between electric and magnetic multipolar order and carrier dynamics (Table IV and Fig. 1) that provides a general framework for further fundamental studies and a wide range of applications of multipolar order in complex materials.

For example, antiferromagnetic order is often characterized as a static spin density wave $\mathbf{S}(\mathbf{q})$ with a finite wave vector \mathbf{q} [105, 106]. Similarly, antiferroelectric order can be viewed as an electric dipolarization density wave $\mathbf{P}(\mathbf{q})$ with $\mathbf{q} \neq 0$. The electric and magnetic multipole densities with $\ell \geq 1$ discussed here represent macroscopic *homogeneous* quantities corresponding to $\mathbf{q} = 0$, like any field and material tensors characterized by Neumann's principle [8]. Beyond spin density waves $\mathbf{S}(\mathbf{q})$ and dipolarization density waves $\mathbf{P}(\mathbf{q})$ ($\ell = 1$), we may envision electric and magnetic multipole density waves $\mathbf{m}(\mathbf{q})$

TABLE XIV. Maximal translationengleiche subgroups of the space group D_{6h}^4 of lonsdaleite and O_h^7 of diamond [37], their crystal classes G , and the lowest orders $\ell_{\min}^{(e,g)}$ ($\ell_{\min}^{(e,u)}$) of even (odd) electric multipole densities these space groups support [45].

space group	G	$\ell_{\min}^{(e,g)}$	$\ell_{\min}^{(e,u)}$	
D_{6h}^4 194 $P6_3/mmc$	$D_{6h} = D_6 \times C_i$	2		lonsdaleite
D_{3h}^4 190 $P\bar{6}2c$	D_{3h}	2	3	
D_{3h}^1 187 $P\bar{6}m2$	D_{3h}	2	3	
C_{6v}^4 186 $P6_3mc$	C_{6v}	2	1	wurtzite
D_6^6 182 $P6_322$	D_6	2	7	(chiral)
C_{6h}^2 176 $P6_3/m$	$C_{6h} = C_6 \times C_i$	2		
D_{3d}^3 164 $P\bar{3}m1$	$D_{3d} = D_3 \times C_i$	2		
D_{3d}^2 163 $P\bar{3}1c$	$D_{3d} = D_3 \times C_i$	2		
D_{2h}^{17} 63 $Cmcm$	$D_{2h} = D_2 \times C_i$	2		
O_h^7 227 $Fd\bar{3}m$	$O_h = O \times C_i$	4		diamond
T_d^2 216 $F\bar{4}3m$	T_d	4	3	zincblende
O^4 210 $F4_132$	O	4	9	(chiral)
T_h^4 203 $Fd\bar{3}$	T_h	4	3	
D_{4h}^{19} 141 $I4_1/amd$	$D_{4h} = D_4 \times C_i$	2		
D_{3d}^5 166 $R\bar{3}m$	$D_{3d} = D_3 \times C_i$	2		

with $\ell > 1$ and $\mathbf{q} \neq 0$. As it is the case for spin density waves $\mathbf{S}(\mathbf{q})$ [105], static waves $\mathbf{m}(\mathbf{q})$ may, but need not, be commensurate with the underlying crystal structure. Electric and magnetic order can be characterized by magnetic point groups if the order is commensurate with the underlying crystal structure. Polarization waves $\mathbf{m}(\mathbf{q})$ for $\ell > 1$ can also represent a generalization of magnons in ferromagnets [106] and ferrons in ferroelectrics [107].

We have illustrated our general theory by considering multipolar order in crystal structures derived from lons-

daleite (Sec. III) and diamond (Sec. IV). Electric and magnetic multipole densities of different order ℓ yield crystallographic point groups as summarized in Table III. Generally, these multipole densities reduce the crystal symmetry of pristine lonsdaleite and diamond. To discuss the same physics from a different perspective, one can start from the space group symmetry of the pristine material and consider its different subgroups. Table XIV lists the maximal translationengleiche subgroups of the space group of pristine lonsdaleite (D_{6h}^4 , No. 194) and diamond (O_h^7 , No. 227) [37]. For each of these subgroups, we list the associated crystal class G and the lowest orders $\ell_{\min}^{(e,g)}$ ($\ell_{\min}^{(e,u)}$) of even (odd) electric multipole densities [45] permitted by these groups. Beyond the space groups already discussed in Secs. III and IV, this list includes also the space groups D_6^6 (No. 182, $P6_322$) and O^4 (No. 210, $F4_132$) that belong to the chiral crystal classes D_6 and O , respectively. Chiral systems do not distinguish between polar vectors like wave vector \mathbf{k} and axial vectors like spin $\boldsymbol{\sigma}$ [108]. Thus it follows immediately that odd- ℓ electric multipole densities in chiral systems manifest themselves via Dirac terms $\propto \boldsymbol{\sigma} \cdot \mathbf{k}$ (that may decompose into separate terms $\propto \sigma_j k_j$ if the system is not cubic).

The group-theoretical tools underlying our analysis can be integrated into crystallographic and materials databases to facilitate materials research. A systematic study of all 122 magnetic crystal classes will be published elsewhere.

ACKNOWLEDGMENTS

RW and UZ acknowledge stimulating discussions with R. Resta and N. Spaldin. RW also benefited from discussions with A. Hoffmann and M. Norman. Work at Argonne was supported by DOE BES under Contract No. DE-AC02-06CH11357.

-
- [1] R. Resta, Macroscopic polarization in crystalline dielectrics: the geometric phase approach, *Rev. Mod. Phys.* **66**, 899 (1994).
 - [2] R. Resta, Electrical polarization and orbital magnetization: the modern theories, *J. Phys.: Condens. Matter* **22**, 123201 (2010).
 - [3] R. M. Martin, Comment on calculations of electric polarization in crystals, *Phys. Rev. B* **9**, 1998 (1974).
 - [4] R. D. King-Smith and D. Vanderbilt, Theory of polarization of crystalline solids, *Phys. Rev. B* **47**, 1651 (1993).
 - [5] R. Resta, Electrical polarization and orbital magnetization: The position operator tamed, in *Handbook of Materials Modeling: Methods: Theory and Modeling*, Vol. 1, edited by W. Andreoni and S. Yip (Springer, Cham, 2020) 2nd ed., Chap. 8, pp. 151–181.
 - [6] J. Gliozzi, M. Lin, and T. L. Hughes, Orbital magnetic quadrupole moment in higher order topological phases, [arXiv:2211.08438](https://arxiv.org/abs/2211.08438) (2022).
 - [7] W. Voigt, *Lehrbuch der Kristallphysik* (B. G. Teubner, Leipzig, 1910).
 - [8] J. F. Nye, *Physical Properties of Crystals* (Oxford University Press, Oxford, 1985).
 - [9] D. B. Litvin, Ferroelectric space groups, *Acta Cryst. A* **42**, 44 (1986).
 - [10] B. A. Tavger and V. M. Zaitsev, Magnetic symmetry of crystals, *Sov. Phys. JETP* **3**, 430 (1956).
 - [11] B. A. Tavger, The symmetry of ferromagnetics and antiferromagnetics, *Sov. Phys. Cryst.* **3**, 341 (1958).
 - [12] Y. Le Corre, Les groupes cristallographiques magnétiques et leurs propriétés, *J. Phys. Radium* **19**, 750 (1958).
 - [13] W. Ludwig and C. Falter, *Symmetries in Physics*, 2nd ed. (Springer, Berlin, 1996).

- [14] H. Watanabe and Y. Yanase, Group-theoretical classification of multipole order: Emergent responses and candidate materials, *Phys. Rev. B* **98**, 245129 (2018).
- [15] S. Hayami, M. Yatsushiro, Y. Yanagi, and H. Kusunose, Classification of atomic-scale multipoles under crystallographic point groups and application to linear response tensors, *Phys. Rev. B* **98**, 165110 (2018).
- [16] M. Yatsushiro, H. Kusunose, and S. Hayami, Multipole classification in 122 magnetic point groups for unified understanding of multiferroic responses and transport phenomena, *Phys. Rev. B* **104**, 054412 (2021).
- [17] S. Bhowal, S. P. Collins, and N. A. Spaldin, Hidden k -space magnetoelectric multipoles in nonmagnetic ferroelectrics, *Phys. Rev. Lett.* **128**, 116402 (2022).
- [18] S. Bhowal and N. A. Spaldin, Magnetic octupoles as the order parameter for unconventional antiferromagnetism, [arXiv:2212.03756](https://arxiv.org/abs/2212.03756) (2022).
- [19] P. Santini, S. Carretta, G. Amoretti, R. Caciuffo, N. Magnani, and G. H. Lander, Multipolar interactions in f -electron systems: The paradigm of actinide dioxides, *Rev. Mod. Phys.* **81**, 807 (2009).
- [20] Y. Kuramoto, H. Kusunose, and A. Kiss, Multipole orders and fluctuations in strongly correlated electron systems, *J. Phys. Soc. Jpn.* **78**, 072001 (2009).
- [21] L. Fu, Parity-breaking phases of spin-orbit-coupled metals with gyrotropic, ferroelectric, and multipolar orders, *Phys. Rev. Lett.* **115**, 026401 (2015).
- [22] M. R. Norman, Dichroism as a probe for parity-breaking phases of spin-orbit coupled metals, *Phys. Rev. B* **92**, 075113 (2015).
- [23] S. Hayami, Y. Yanagi, H. Kusunose, and Y. Motome, Electric toroidal quadrupoles in the spin-orbit-coupled metal $\text{Cd}_2\text{Re}_2\text{O}_7$, *Phys. Rev. Lett.* **122**, 147602 (2019).
- [24] S. Voleti, A. Haldar, and A. Paramakanti, Octupolar order and Ising quantum criticality tuned by strain and dimensionality: Application to d -orbital Mott insulators, *Phys. Rev. B* **104**, 174431 (2021).
- [25] M. Tahir and H. Chen, Current-induced quasiparticle magnetic multipole moments, [arXiv:2210.15753](https://arxiv.org/abs/2210.15753) (2022).
- [26] M. Posternak, A. Baldereschi, A. Catellani, and R. Resta, *Ab initio* study of the spontaneous polarization of pyroelectric BeO, *Phys. Rev. Lett.* **64**, 1777 (1990).
- [27] F. Bernardini, V. Fiorentini, and D. Vanderbilt, Spontaneous polarization and piezoelectric constants of III-V nitrides, *Phys. Rev. B* **56**, R10024 (1997).
- [28] E. I. Rashba and V. I. Sheka, Symmetry of energy bands in crystals of wurtzite type: II. symmetry of bands including spin-orbit interaction, *Fiz. Tverd. Tela: Collected Papers* **2**, 162 (1959), for an English translation, see the supplement of G. Bihlmayer, O. Rader, and R. Winkler, Focus on the Rashba effect, *New J. Phys.* **17**, 050202 (2015).
- [29] E. I. Rashba, Spin-orbit coupling and spin transport, *Physica E* **34**, 31 (2006).
- [30] R. Lassnig, $\mathbf{k} \cdot \mathbf{p}$ theory, effective-mass approach, and spin splitting for two-dimensional electrons in GaAs-GaAlAs heterostructures, *Phys. Rev. B* **31**, 8076 (1985).
- [31] R. Winkler, *Spin-Orbit Coupling Effects in Two-Dimensional Electron and Hole Systems* (Springer, Berlin, 2003).
- [32] L. C. Lew Yan Voon, M. Willatzen, M. Cardona, and N. E. Christensen, Terms linear in k in the band structure of wurtzite-type semiconductors, *Phys. Rev. B* **53**, 10703 (1996).
- [33] G. Dresselhaus, Spin-orbit coupling effects in zinc blende structures, *Phys. Rev.* **100**, 580 (1955).
- [34] J. D. Jackson, *Classical Electrodynamics*, 3rd ed. (Wiley, New York, 1999).
- [35] R. E. Raab and O. L. de Lange, *Multipole Theory in Electromagnetism* (Clarendon, Oxford, 2005).
- [36] Y. Kuramoto, Electronic higher multipoles in solids, *Prog. Theor. Phys. Suppl.* **176**, 77 (2008).
- [37] T. Hahn, ed., *International Tables for Crystallography*, 5th ed., Vol. A (Springer, Dordrecht, 2005).
- [38] D. B. Litvin, *Magnetic Group Tables*, Tech. Rep. (International Union of Crystallography, 2013).
- [39] Y. A. Artamonov and A. A. Gorbatshevich, Symmetry and dynamics of systems with toroidal moments, *Zh. Eksp. Teor. Fiz.* **89**, 1078 (1985), [*Sov. Phys. JETP* **62**, 621 (1985)].
- [40] V. M. Dubovik and V. V. Tugushev, Toroid moments in electrodynamics and solid-state physics, *Phys. Rep.* **187**, 145 (1990).
- [41] N. A. Spaldin, M. Fiebig, and M. Mostovoy, The toroidal moment in condensed-matter physics and its relation to the magnetoelectric effect, *J. Phys.: Condens. Matter* **20**, 434203 (2008).
- [42] N. Papasimakis, V. A. Fedotov, V. Savinov, T. A. Raybould, and N. I. Zheludev, Electromagnetic toroidal excitations in matter and free space, *Nat. Mater.* **15**, 263 (2016).
- [43] S. Nanz, *Toroidal Multipole Moments in Classical Electrodynamics* (Springer, Wiesbaden, 2016).
- [44] I. Fernandez-Corbaton, S. Nanz, and C. Rockstuhl, On the dynamic toroidal multipoles from localized electric current distributions, *Sci. Rep.* **7**, 7527 (2017).
- [45] G. F. Koster, J. O. Dimmock, R. G. Wheeler, and H. Statz, *Properties of the Thirty-Two Point Groups* (MIT, Cambridge, MA, 1963).
- [46] L. D. Landau and E. M. Lifshitz, *Electrodynamics of Continuous Media*, 2nd ed. (Pergamon, Oxford, 1984).
- [47] J. Oitmaa, Diamond lattice Heisenberg antiferromagnet, *J. Phys.: Condens. Matter* **30**, 155801 (2018).
- [48] Electric and magnetic multipoles can also be viewed as cartesian rank- ℓ tensors [34, 35]. However, as is well-known [49], spherical rank- ℓ tensors transform irreducibly under the rotation group $R_{i \times \theta}$, whereas cartesian tensors of rank $\ell \geq 2$ are reducible, which is the reason why we prefer to define electric and magnetic multipoles as spherical tensors and not as cartesian tensors.
- [49] A. R. Edmonds, *Angular Momentum in Quantum Mechanics*, 2nd ed. (Princeton University Press, Princeton, 1960).
- [50] W.-K. Tung, *Group Theory in Physics* (World Scientific, Singapore, 1985).
- [51] G. Herzberg, *Molecular Spectra and Molecular Structure* (Van Nostrand, New York, 1950).
- [52] G. L. Bir and G. E. Pikus, *Symmetry and Strain-Induced Effects in Semiconductors* (Wiley, New York, 1974).
- [53] C. J. Bradley and A. P. Cracknell, *The Mathematical Theory of Symmetry in Solids* (Clarendon, Oxford, 1972).
- [54] This classification is not exhaustive, see Sec. V.
- [55] R. E. Newnham, *Properties of Materials* (Oxford University Press, New York, 2005).
- [56] R. F. Tinder, *Tensor Properties of Solids* (Morgan and

- Claypool, San Rafael, CA, 2008).
- [57] R. R. Birss, *Symmetry and Magnetism* (North-Holland, Amsterdam, Netherlands, 1964).
- [58] Systems transforming according to so-called type-IV magnetic space groups [53] possess a black-and-white Bravais lattice. These are antiferromagnetic systems that belong to a nonmagnetic crystal class [12, 57], and they are parapolar or electropolar according to the present classification. All systems studied in the present work have type-II or type-III magnetic space groups.
- [59] M. Fiebig, T. Lottermoser, D. Meier, and M. Trassin, The evolution of multiferroics, *Nat. Rev. Mater.* **1**, 16046 (2016).
- [60] N. A. Spaldin, Multiferroics: Past, present, and future, *MRS Bulletin* **42**, 385 (2017).
- [61] Compatibility relations for the crystallographic point groups were introduced by L. P. Bouckaert, R. Smoluchowski, and E. Wigner, *Phys. Rev.* **50**, 58 (1936).
- [62] The isomorphisms between magnetic and nonmagnetic crystallographic point groups exist at the level of the single (spinless) groups relevant, e.g., for Neumann's principle. Only at the level of double groups, these groups are generally not isomorphic because then $i^2 = e$, whereas $\theta^2 = \bar{e}$ with $e^2 = e$.
- [63] The compatibility relations relating two crystallographic point groups G and U are not uniquely defined. They depend on the relative orientation of the coordinate systems used to define the symmetry operations in G and U .
- [64] These considerations can be extended to include, e.g., the possibility that a magnetic phase transition may be accompanied by a structural phase transition. If a nonmagnetic structure undergoes a phase transition to a magnetic phase, by definition a magnetic multipole becomes allowed. The phase transition may likewise affect the electric order. For example, it is well-known that iron is cubic above the Curie temperature and therefore has an electric hexadecapolarization ($\ell = 4$), but it develops a tetragonal distortion in the ferromagnetic state [106] that allows an electric quadrupolarization ($\ell = 2$).
- [65] J. M. Luttinger, Quantum theory of cyclotron resonances in semiconductors: General theory, *Phys. Rev.* **102**, 1030 (1956).
- [66] R. Winkler and U. Zülicke, Collinear orbital antiferromagnetic order and magnetoelectricity in quasi-two-dimensional itinerant-electron paramagnets, ferromagnets, and antiferromagnets, *Phys. Rev. Research* **2**, 043060 (2020).
- [67] G. Giuliani and G. Vignale, *Quantum Theory of the Electron Liquid* (Cambridge University Press, Cambridge, UK, 2005).
- [68] T. Kjeldaa and W. Kohn, Theory of the diamagnetism of Bloch electrons, *Phys. Rev.* **105**, 806 (1957).
- [69] L. M. Roth, B. Lax, and S. Zwerdling, Theory of optical magneto-absorption effects in semiconductors, *Phys. Rev.* **114**, 90 (1959).
- [70] R. Resta, M. Posternak, and A. Baldereschi, Towards a quantum theory of polarization in ferroelectrics: The case of KNbO_3 , *Phys. Rev. Lett.* **70**, 1010 (1993).
- [71] D. Ceresoli, T. Thonhauser, D. Vanderbilt, and R. Resta, Orbital magnetization in crystalline solids: Multi-band insulators, chern insulators, and metals, *Phys. Rev. B* **74**, 024408 (2006).
- [72] J. Shi, G. Vignale, D. Xiao, and Q. Niu, Quantum theory of orbital magnetization and its generalization to interacting systems, *Phys. Rev. Lett.* **99**, 197202 (2007).
- [73] N. O. Lipari and A. Baldereschi, Angular momentum theory and localized states in solids: Investigation of shallow acceptor states in semiconductors, *Phys. Rev. Lett.* **25**, 1660 (1970).
- [74] H.-R. Trebin, U. Rössler, and R. Ranvaud, Quantum resonances in the valence bands of zinc-blende semiconductors. I. Theoretical aspects, *Phys. Rev. B* **20**, 686 (1979).
- [75] See, e.g., L. Bellaiche and D. Vanderbilt, *Phys. Rev. B* **61**, 7877 (2000), and references therein.
- [76] K. Suzuki and J. C. Hensel, Quantum resonances in the valence bands of germanium. I. Theoretical considerations, *Phys. Rev. B* **9**, 4184 (1974).
- [77] L.-D. Yuan, Z. Wang, J.-W. Luo, and A. Zunger, Prediction of low-Z collinear and noncollinear antiferromagnetic compounds having momentum-dependent spin splitting even without spin-orbit coupling, *Phys. Rev. Materials* **5**, 014409 (2021).
- [78] L. Šmejkal, J. Sinova, and T. Jungwirth, Beyond conventional ferromagnetism and antiferromagnetism: A phase with nonrelativistic spin and crystal rotation symmetry, *Phys. Rev. X* **12**, 031042 (2022).
- [79] L. Šmejkal, J. Sinova, and T. Jungwirth, Emerging research landscape of altermagnetism, *Phys. Rev. X* **12**, 040501 (2022).
- [80] This discussion also applies to magnetic monopoles and axions transforming according to D_0^- of $R_{i \times \theta}$. These quantities are forbidden by $R_{i \times \theta}$ in vacuum but are symmetry-allowed by 32 of the 122 magnetic crystallographic point groups.
- [81] H. T. Stokes and D. M. Hatch, FINDSYM: program for identifying the space-group symmetry of a crystal, *J. Appl. Cryst.* **38**, 237 (2005).
- [82] R. A. Evarestov and V. P. Smirnov, *Site Symmetry in Crystals*, 2nd ed. (Springer, Berlin, 1997).
- [83] E. A. Fajardo and R. Winkler, Effective dynamics of two-dimensional Bloch electrons in external fields derived from symmetry, *Phys. Rev. B* **100**, 125301 (2019).
- [84] G. Burns and A. M. Glazer, *Space Groups for Solid State Scientists*, 3rd ed. (Academic, Amsterdam, 2013).
- [85] N. A. Spaldin, M. Fechner, E. Bousquet, A. Balatsky, and L. Nordström, Monopole-based formalism for the diagonal magnetoelectric response, *Phys. Rev. B* **88**, 094429 (2013).
- [86] E. I. Rashba, Symmetry of energy bands in crystals of wurtzite type: I. symmetry of bands disregarding spin-orbit interaction, *Sov. Phys.-Solid State* **1**, 368 (1959).
- [87] Beyond the invariant (13), the Hamiltonian for Bloch electrons in lonsdaleite also includes a spherically symmetric invariant that transforms according to D_0^+ of R_i so that it transforms according to Γ_1 of any subgroup of R_i
- $$H^{(e,0)} = a^{(e,0)} m^{(e,0)} (k_x^2 + k_y^2 + k_z^2).$$
- Thus, instead of $H^{(e,0)}$ and $H^{(e,2)}$, we could also choose for D_{6h} the linearly independent invariants
- $$H_{xy}^{(e,2)} = b_{xy}^{(e,2)} (k_x^2 + k_y^2), \quad H_z^{(e,2)} = b_z^{(e,2)} k_z^2,$$
- with
- $$b_{xy}^{(e,2)} = a^{(e,0)} m^{(e,0)} + a^{(e,2)} m^{(e,2)}$$

$$b_z^{(e,2)} = a^{(e,0)} m^{(e,0)} - 2a^{(e,2)} m^{(e,2)}.$$

However, both $k_x^2 + k_y^2$ and k_z^2 already have nonvanishing expectation values under R_i , whereas the expectation value of $K_1^{(e,2)}$ vanishes under R_i . Therefore $I_1^{(e,2)} \propto K_1^{(e,2)}$ constitutes the indicator for the electric quadrupole density in lonsdaleite.

- [88] J. J. Sinai, Octopole moment of methane, *J. Chem. Phys.* **40**, 3596 (1964).
- [89] A. Kobayashi, O. F. Sankey, S. M. Volz, and J. D. Dow, Semiempirical tight-binding band structures of wurtzite semiconductors: AlN, CdS, CdSe, ZnS, and ZnO, *Phys. Rev. B* **28**, 935 (1983).
- [90] L.-D. Yuan, Z. Wang, J.-W. Luo, E. I. Rashba, and A. Zunger, Giant momentum-dependent spin splitting in centrosymmetric low- Z antiferromagnets, *Phys. Rev. B* **102**, 014422 (2020).
- [91] M. Tinkham, *Group Theory and Quantum Mechanics* (McGraw-Hill, New York, 1964).
- [92] E. O. Kane, Band structure of indium antimonide, *J. Phys. Chem. Solids* **1**, 249 (1957).
- [93] U. Rössler, Nonparabolicity and warping in the conduction band of GaAs, *Solid State Commun.* **49**, 943 (1984).
- [94] D. J. Chadi and M. L. Cohen, Tight-binding calculations of the valence bands of diamond and zincblende crystals, *phys. stat. sol. (b)* **68**, 405 (1975).
- [95] D. J. Chadi, Spin-orbit splitting in crystalline and compositionally disordered semiconductors, *Phys. Rev. B* **16**, 790 (1977).
- [96] M. Cardona, N. E. Christensen, and G. Fasol, Relativistic band structure and spin-orbit splitting of zincblende-type semiconductors, *Phys. Rev. B* **38**, 1806 (1988).
- [97] L. D. Landau and E. M. Lifshitz, *Theory of Elasticity*, 3rd ed. (Pergamon, Oxford, 1987).
- [98] M. I. D'yakonov and V. Y. Kachorovskii, Spin relaxation of two-dimensional electrons in noncentrosymmetric semiconductors, *Sov. Phys.-Semicond.* **20**, 110 (1986).
- [99] X. Cartoixà, D. Z.-Y. Ting, and Y.-C. Chang, Suppression of the D'yakonov-Perel' spin-relaxation mechanism for all spin components in [111] zincblende quantum wells, *Phys. Rev. B* **71**, 045313 (2005).
- [100] H. Watanabe and Y. Yanase, Magnetic hexadecapole order and magnetopiezoelectric metal state in $\text{Ba}_{1-x}\text{K}_x\text{Mn}_2\text{As}_2$, *Phys. Rev. B* **96**, 064432 (2017).
- [101] The configuration shown in Fig. 4(e) is the classic diamond-lattice antiferromagnet [47]. Another example of magnetic quadrupolar order is discussed in Ref. [109].
- [102] T. Dietl and H. Ohno, Dilute ferromagnetic semiconductors: Physics and spintronic structures, *Rev. Mod. Phys.* **86**, 187 (2014).
- [103] A. Manchon, H. C. Koo, J. Nitta, S. M. Frolov, and R. A. Duine, New perspectives for Rashba spin-orbit coupling, *Nat. Mater.* **14**, 871 (2015).
- [104] H. Djani, A. C. Garcia-Castro, W.-Y. Tong, P. Barone, E. Bousquet, S. Picozzi, and P. Ghosez, Rationalizing and engineering Rashba spin-splitting in ferroelectric oxides, *npj Quantum Mater.* **4**, 51 (2019).
- [105] C. Herring, *Exchange Interaction among Itinerant Electrons*, edited by G. T. Rado and H. Suhl, Magnetism, Vol. IV (Academic, New York, 1966).
- [106] R. M. White, *Quantum Theory of Magnetism*, 3rd ed. (Springer, Berlin, 2007).
- [107] G. E. W. Bauer, P. Tang, R. Iguchi, and K. Uchida, Magnonics vs. ferronics, *J. Magn. Magn. Mater.* **541**, 168468 (2022).
- [108] L. D. Barron, *Molecular Light Scattering and Optical Activity*, 2nd ed. (Cambridge University Press, Cambridge, UK, 2004).
- [109] S. Hayami, H. Kusunose, and Y. Motome, Emergent odd-parity multipoles and magnetoelectric effects on a diamond structure: Implication for the 5d transition metal oxides AOsO_4 ($A = \text{K, Rb, and Cs}$), *Phys. Rev. B* **97**, 024414 (2018).